# Chapter 3
# Recent Variability in Sea Ice Cover, Age, and Thickness in the Pacific Arctic Region

**Karen E. Frey, James A. Maslanik, Jaclyn Clement Kinney, and Wieslaw Maslowski**

**Abstract** Over the past several decades, there has been a fundamental shift in sea ice cover, age, and thickness across the Pacific Arctic Region (PAR). Satellite data reveal that trends in sea ice cover have been spatially heterogeneous, with significant declines in the Chukchi Sea, slight declines in the Bering Strait region, yet increases in the northern Bering Sea south of St. Lawrence Island. Declines in the annual persistence of seasonal sea ice cover in the Chukchi Sea and Bering Strait region are due to both earlier sea ice breakup and later sea ice formation. However, increases in the persistence of seasonal sea ice cover south of St. Lawrence Island occur primarily owing to earlier sea ice formation during winter months. Satellite-based observations of sea ice age along with modeled sea ice thickness provide further insight into recent sea ice variability throughout the PAR, with widespread transitions towards younger, thinner ice. Investigation of sea ice cover, age, and thickness in concert provides critical insight into ongoing changes in the total volume of ice and therefore the future trajectory of sea ice throughout the PAR, as well as its likely impacts on ecosystem productivity across all trophic levels.

**Keywords** Sea ice • Bering Sea • Chukchi Sea • Sea ice age • Sea ice thickness • Satellite data

K.E. Frey (✉)
Graduate School of Geography, Clark University, Worcester, MA 01610, USA
e-mail: kfrey@clarku.edu

J.A. Maslanik
Colorado Center for Astrodynamics Research, University of Colorado, Boulder, CO 80309, USA

J. Clement Kinney • W. Maslowski
Department of Oceanography, Graduate School of Engineering and Applied Sciences, Naval Postgraduate School, Dyer Road, Bldg. SP339B, Monterey, CA 93943, USA
e-mail: jlclemen@nps.edu; maslowsk@nps.edu

J.M. Grebmeier and W. Maslowski (eds.), *The Pacific Arctic Region: Ecosystem Status and Trends in a Rapidly Changing Environment*, DOI 10.1007/978-94-017-8863-2_3,

## 3.1 Introduction

The Arctic Ocean has experienced significant warming (Zhang 2005; Polyakov et al. 2007; Steele et al. 2008) and dramatic declines in sea ice over the past few decades (Parkinson et al. 1999; Cavalieri et al. 2003; Serreze et al. 2003; Stroeve et al. 2005, 2008, 2012). These reductions in sea ice have facilitated a positive feedback through decreased albedo and enhanced absorption of solar insolation (e.g., Perovich et al. 2007), leading to model predictions of a near absence of summer sea ice by the year 2040 (Holland et al. 2006) and possibly sooner (Stroeve et al. 2007; Wang and Overland 2009). Although significant sea ice declines have been observed for all months, seasonal sea ice minima in September have been particularly striking (Stroeve et al. 2008; Perovich et al. 2011). Key factors in the declines in sea ice cover include long-term thinning trends of sea ice and replacement of thick, multi-year ice with thin, first-year ice (Nghiem et al. 2007; Maslanik et al. 2007a, 2011). These reductions are exacerbated by increased heat fluxes entering the Chukchi Sea through Bering Strait (Shimada et al. 2006; Woodgate et al. 2006), leading to ocean warming that in turn delays autumn sea ice re-growth (Steele et al. 2008). Reductions in Arctic sea ice cover have been most pronounced in the marginal seas of the Alaskan and Russian continental shelves, including areas in the Pacific Arctic Region (PAR) (Steele et al. 2008; Stroeve et al. 2012) that are the focus of the chapters in this book.

In the context of the overriding theme of this book, it is important to consider the potential impacts of recent sea ice variability on ecosystem productivity throughout the PAR. Sea ice melt and breakup during spring strongly impact primary production in the Arctic Ocean and its adjacent shelf seas by enhancing light availability as well as increasing stratification and stabilization of the water column. Recently observed declines in sea ice extent, thickness, and annual persistence should therefore have important consequences for primary production throughout the PAR. Recent studies indeed document significant increases in primary production in several sectors of the Arctic Ocean, in addition to significant shifts in the timing of phytoplankton blooms. For example, newly compiled satellite observations of primary production in the Arctic Ocean over a 12-year period (1998–2009) reveal a ~20 % overall increase, resulting primarily from increases in open water extent (+27 %) and duration of the open water season (+45 days) (Arrigo and van Dijken 2011). Enhanced light availability through increasingly melt-ponded sea ice surfaces (Frey et al. 2011) can also contribute to high levels of primary production underneath the ice (Arrigo et al. 2012). Furthermore, Kahru et al. (2010) found significant trends towards earlier phytoplankton blooms for ~11 % of the Arctic Ocean over the 1997–2009 period in areas roughly coincident with those experiencing earlier sea ice breakup.

Although general increases in primary production are predicted to accompany continuing losses in sea ice cover, shifts in primary production are expected to be spatially heterogeneous and dependent on several potentially confounding factors. For instance, models presented by Slagstad et al. (2011) suggest that while some

Arctic shelf areas may have significant increases in primary production with further sea ice declines, the deep central basin of the Arctic Ocean may see smaller increases in production owing to low nutrient concentrations, areas that lose all ice cover may see decreases in production owing to increased stratification with atmospheric warming, and some inner coastal shelves may see little increase in production owing to the enhanced turbidity from river runoff and coastal erosion. Empirically-based extrapolations presented by Arrigo and van Dijken (2011) suggest that when summer ice cover falls to zero, total annual primary production could reach ~730 Tg C $year^{-1}$ total across the Arctic (a ~48 % increase over the 1998–2009 average). However, this value is highly dependent upon future distributions of nutrients, the extent of warming-induced enhanced stratification, and other limitations to primary production such as river-associated turbidity in coastal regions.

In this chapter, we investigate the variability and trends in sea ice physical characteristics across the PAR (Sect. 3.1) over the past several decades, providing a physical context for the ecosystem-centric chapters in this book. The PAR has experienced some of the most dramatic shifts in sea ice of any region across the pan-Arctic. Quantifying changes in sea ice cover, age, and thickness combined provides an assessment of overall trends sea ice volume, thereby garnering important insights into the potential future trajectory of sea ice conditions and potential impacts on ecosystem productivity. In Sect. 3.2 we focus on trends and recent interannual variability of sea ice cover (including the seasonal duration of ice cover, timing of breakup, and timing of formation) based on passive microwave satellite observations. In Sect. 3.3, we focus on changes in the age of sea ice derived from satellite observations blended with drifting-buoy vectors. In Sect. 3.4 we estimate changes in of sea ice thickness in the PAR based on a pan-Arctic coupled ice-ocean model. Lastly, in Sect. 3.5, we provide a discussion of the implications and possible future states of sea ice throughout the PAR.

## 3.2 Sea Ice Cover

### *3.2.1 Trends in Sea Ice Cover*

The sea ice cover in the PAR is highly seasonally variable, with much of the northern Bering and Chukchi seas covered with first-year sea ice for several winter months of each year. Northern portions of the Chukchi Sea have also contained variable amounts of multiyear sea ice (i.e., ice that has survived at least one melt season) over the last several decades of the observed satellite record. In order to investigate trends in sea ice cover throughout the PAR over the last several decades, sea ice concentrations (spanning the years 1979–2008) derived from the Scanning Multichannel Microwave Radiometer (SMMR) and Special Sensor Microwave/Imager (SSM/I) passive microwave instruments (Cavalieri et al. 2008) were utilized for this study. These data are available at a 25 km spatial resolution, where the

SSM/I data are daily and the SMMR data are available every other day (but were temporally interpolated to create a daily time series). As is standard in most studies, we used a 15 % ice concentration threshold to define the presence vs. absence of sea ice cover for calculations of sea ice extent.

Positions of the median sea ice edge for the last three decades (1979–1988, 1989–1998, and 1999–2008) for both March (seasonal sea ice maximum) and September (seasonal sea ice minimum) are shown in Sect. 3.1. Substantial shifts in sea ice cover throughout the PAR over the last 30 years of the satellite record are clearly evident. For March, the sea ice edge advanced slightly southward during 1989–1998 compared with its position during 1979–1998. However, the March ice edge during 1999–2008 was at its northernmost position of the three decades. In contrast, the position of the September ice edge has shifted dramatically and systematically northward over the last three decades. During 1979–1988, the median September edge was so far south that it barely retreated off the Siberian coast, was nearly coincident with the shelf break in the Beaufort Sea, and only partially exposed the Chukchi Sea shelf. Two decades later, during 1999–2008, the median September ice edge was positioned far north of the coasts, exposing the deep Arctic Ocean basin in the eastern PAR.

Trends in areal coverage of sea ice in the northern Bering and Chukchi Seas were also quantified over the satellite record from 1979 to 2008 (Figs. 3.2 and 3.3). In this case, the northern Bering Sea is defined as the shelf area north of St. Matthew Island to Bering Strait, whereas the Chukchi Sea is defined as the shelf area north of the Bering Strait between Wrangel Island and Barrow Canyon (Fig. 3.1). For the Bering Sea, statistically significant trends ($p<0.10$) are found only during the months of June, July, September, October, and November (Sect. 3.2, Table 3.1), with no trend in August owing to the lack of ice cover during that month. During winter and spring, however, sea ice cover in the northern Bering Sea has been highly variable and without trend (Fig. 3.2). In contrast, trends in sea ice cover in the Chukchi Sea have been far more dramatic and statistically significant for all months except April (Fig. 3.3, Table 3.1). During January, February, and March, slight increases in ice cover in the Chukchi Sea have been observed. For May through December, however, all trends show significant declines, where the greatest losses occurred during September: 63,840 km$^2$/decade or 31.8 %/decade.

Seasonal patterns and longer-term shifts in the spatial extent of sea ice were also compared over an annual time span. Daily averaged sea ice extent over 5-year increments exhibit extreme wintertime variability in the northern Bering Sea, with peak extent (~550,000 km$^2$) typically occurring during March and complete loss of seasonal sea ice by June–July (Sect. 3.4). Wintertime sea ice in the Chukchi Sea is comparably stable, with similar peak extent (~550,000 km$^2$) attained by December and spring breakup starting in May. In the Chukchi Sea, sea ice breakup has shifted earlier and ice formation has shifted later over the 30-year satellite record, with sea ice spatial extent substantially reduced during all non-winter months (Fig. 3.4).

The timing of sea ice breakup and formation is also important to consider, where we define the timing of these events as the day of year that sea ice

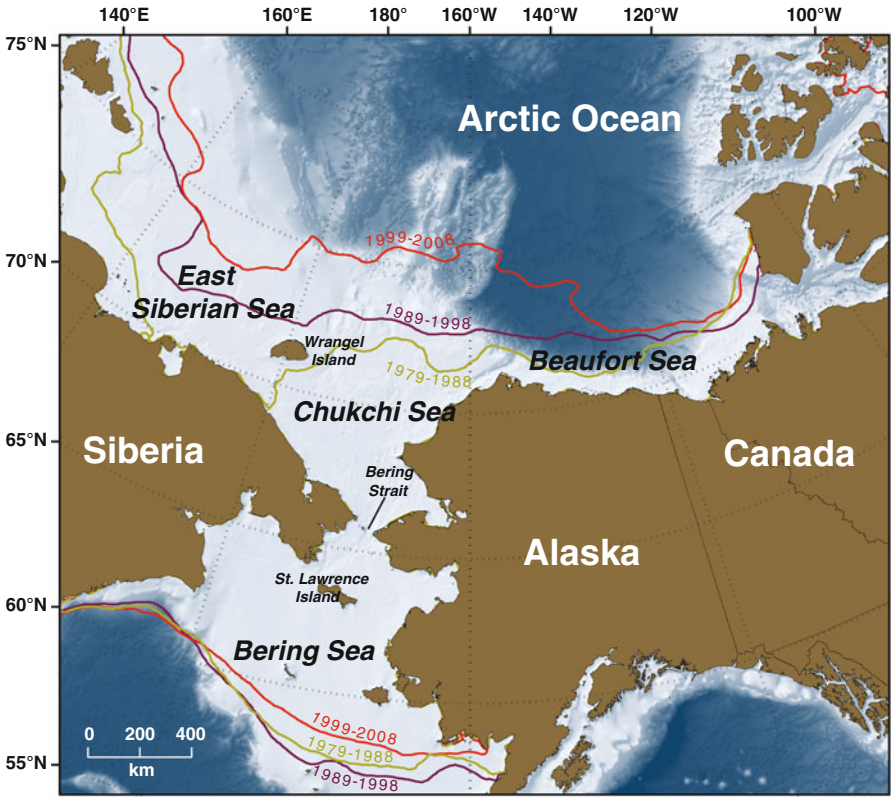


**Fig. 3.1** Location of the Pacific Arctic Region (*PAR*). Isolines (based on SMMR and SSM/I sea ice concentrations) indicate the position of the median sea ice edge (defined by a 15 % sea ice concentration threshold) for 1979–1988, 1989–1998, and 1999–2008 during both March (southern isolines) and September (northern isolines)

concentrations fall below or exceed 15 %, respectively. We also define annual sea ice persistence as the total number of days per year that sea ice concentrations are greater than 15 %. Viewing the persistence and timing of breakup/formation spatially (Fig. 3.5) provides valuable insight into sea ice variability across the past three decades, particularly in the context of seasonally varying and sea ice dependent processes such as biological productivity. The PAR is highly dynamic in terms of annual sea ice persistence, ranging from 0 through >300 days per year of sea ice cover (Fig. 3.5). The timing of sea ice breakup also exhibits a broad range, with the earliest breakup in the Bering Sea (April) and the latest breakup in the northern Chukchi Sea (August–September). Similarly, the timing of sea ice formation is earliest in the northern Chukchi Sea (October–November) and latest in the Bering Sea (January–March). The timing of these events has shifted dramatically over the past three decades, which can be directly and spatially quantified by presenting linear decadal trends of annual sea ice persistence, the timing of sea ice

**Table 3.1** Linear trends of sea ice decline in the northern Bering and Chukchi Seas over the 30 year record (1979–2008). Only those trends that are statistically significant ($p<0.10$) are shown

| | Northern Bering Sea | | Chukchi Sea | |
|---|---|---|---|---|
| | km$^2$/decade | %/decade | km$^2$/decade | %/decade |
| January | | | 4,466 | 1.0 |
| February | | | 5,354 | 1.2 |
| March | | | 3,502 | 0.8 |
| April | | | | |
| May | | | −8,107 | −1.8 |
| June | −2,788 | −8.9 | −24,186 | −6.1 |
| July | −568 | −19.9 | −39,048 | −13.8 |
| August | | | −48,273 | −25.0 |
| September | −726 | −20.0 | −63,840 | −31.8 |
| October | −2,283 | −15.2 | −70,118 | −24.7 |
| November | −7,913 | −13.9 | −48,820 | −12.6 |
| December | | | −13,329 | −2.9 |

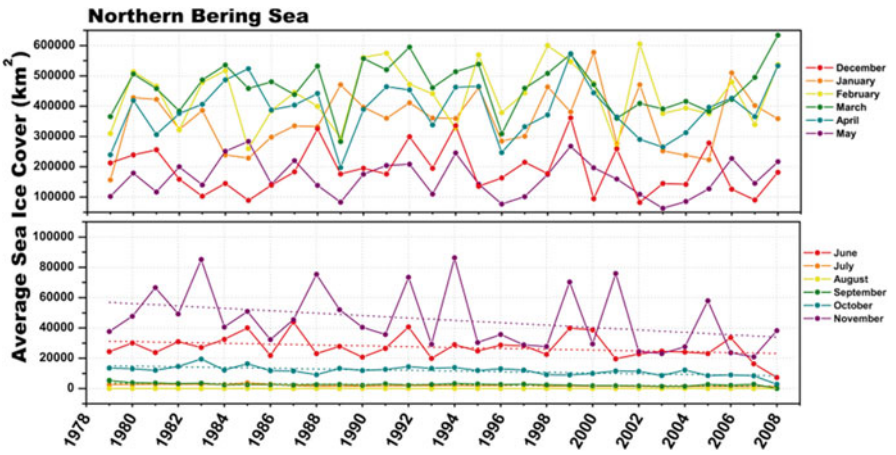


**Fig. 3.2** Average sea ice cover for the northern Bering Sea for each month from 1979 to 2008. Trend lines are shown for only those months showing statistically significant ($p<0.10$) trends (Table 3.1). Results are based on SMMR and SSM/I sea ice concentrations

breakup, and the timing of sea ice formation (Fig. 3.6). The most extreme decadal shifts in sea ice cover have occurred within the central Chukchi Sea, where sea ice persistence has declined by more than 30 days/decade over the 30 year record. Decreased ice persistence was caused by not only earlier sea ice breakup (~10 days/decade earlier), but also later sea ice formation (~20 days/decade later). This reduction in sea ice cover has been pronounced in the Chukchi Sea, but trends lessen moving southward through the Bering Strait into the northern Bering Sea region surrounding St. Lawrence Island. South of St. Lawrence Island, sea ice

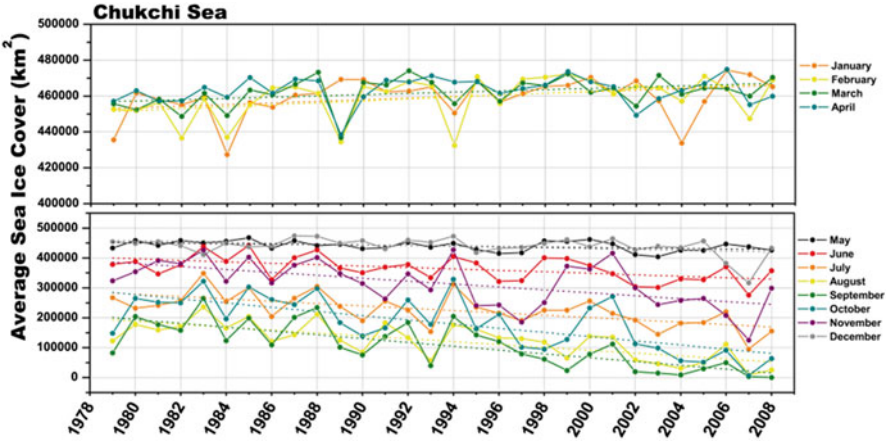


**Fig. 3.3** Average sea ice cover for the Chukchi Sea for each month from 1979 to 2008. Trend lines are shown for only those months showing statistically significant ($p<0.10$) trends (Table 3.1). Results are based on SMMR and SSM/I sea ice concentrations

persistence trends show a slight increase in ice cover, driven more by earlier sea ice formation in winter rather than by later ice breakup in spring.

### *3.2.2 Interannual Variability in Sea Ice Cover*

Sea ice cover was also investigated at a higher spatial resolution (6.25 km) with daily sea ice concentrations derived via the Advanced Microwave Scanning Radiometer for EOS (AMSR-E) sensor on the Aqua satellite platform launched in May 2002 (Spreen et al. 2008). Based on a 15 % sea ice concentration threshold, annual sea ice persistence (Fig. 3.7), the timing of sea ice breakup (Fig. 3.8), and the timing of sea ice formation (Fig. 3.9) were quantified for the PAR with AMSR-E data spanning 2002–2009. Although the time series of AMSR-E data is not long enough to determine statistically significant trends in these parameters, these data nevertheless allow for an investigation of the interannual variability of sea ice cover across the PAR with high spatial detail. Just as with the SMMR and SSM/I data, similar patterns in annual sea ice persistence emerge (Fig. 3.7), with a distinct latitudinal gradient from no sea ice cover south of the ice edge in the Bering Sea to >300 days/year of sea ice cover in the northern Chukchi Sea. Consistent with observations in other studies showing a 2007 minimum in Arctic sea ice extent (e.g., Stroeve et al. 2008), 2007 shows the fewest number of days of sea ice coverage throughout the PAR as a whole over the years 2003–2009. In contrast, however, 2003 and 2004 show the smallest sea ice cover for the Bering Sea specifically, although the position of the winter sea ice edge was farthest north in 2005.

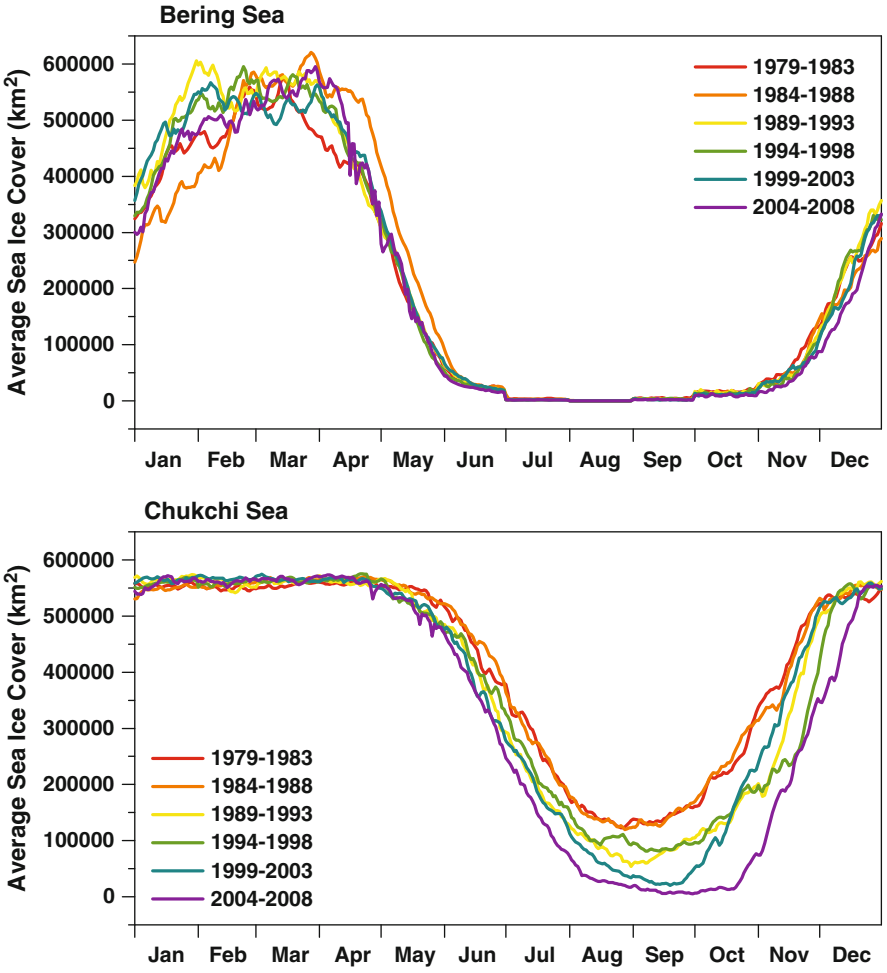


**Fig. 3.4** Daily average sea ice extent for the northern Bering Sea (*top*) and Chukchi Sea (*bottom*) for 5-year periods from 1979 to 2008. Results are based on SMMR and SSM/I sea ice concentrations (using a 15 % sea ice concentration threshold). Overall, the open water season is significantly longer for the northern Bering than for the Chukchi Sea. Shifts towards an earlier seasonal sea ice breakup and later sea ice formation are particularly apparent for the Chukchi Sea

Investigation of the timing of sea ice breakup and sea ice formation additionally illustrates important spatial patterns in these events across the PAR. In general, spatial patterns in sea ice breakup were distinctly spatially heterogeneous (Fig. 3.8), where the timing of sea ice breakup did not necessarily follow an ideal latitudinal gradient. However, ice at the sea ice edge in the Bering Sea generally breaks up first (early March) and advances northward into the Bering Strait by late April-early May. Ice breakup tends to occur relatively early within polynya regions (e.g., south of St. Lawrence Island), which is particularly apparent in 2005, 2006, 2007, and 2008. Ice breakup occurs later in the Chukchi Sea, with ice in the southern Chukchi

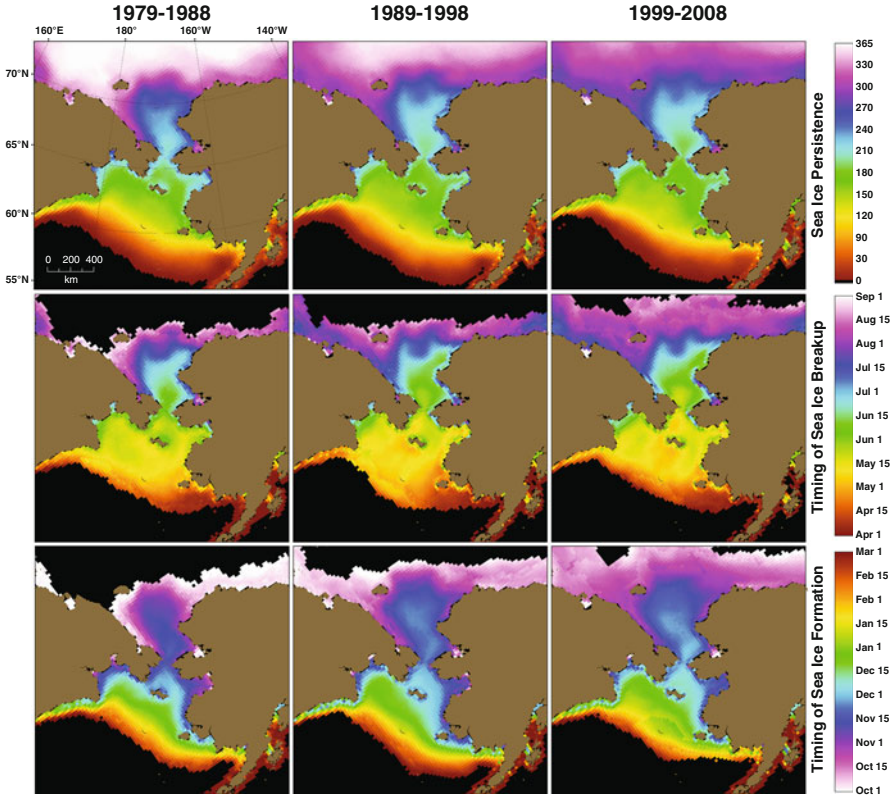


**Fig. 3.5** Average annual sea ice persistence, timing of sea ice breakup, and timing of sea ice formation in the PAR during the past three decades. Results are based on SMMR and SSM/I sea ice concentrations (using a 15 % sea ice concentration threshold)

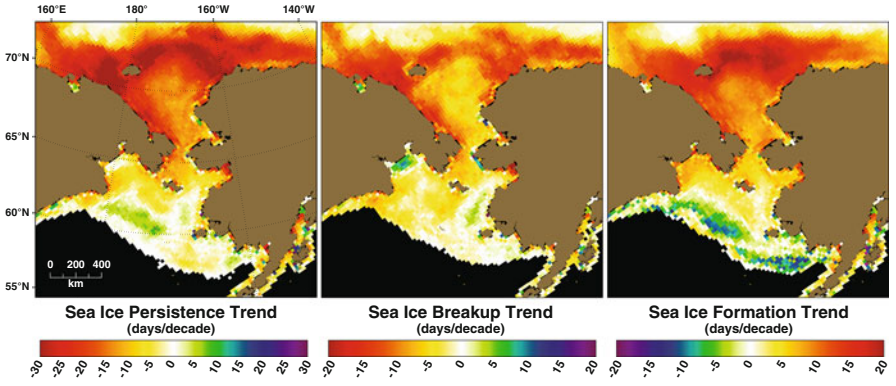


**Fig. 3.6** Linear decadal trends in annual sea ice persistence, sea ice breakup, and sea ice formation over the 1979–2008 period. Results are based on SMMR and SSM/I sea ice concentrations (using a 15 % sea ice concentration threshold)

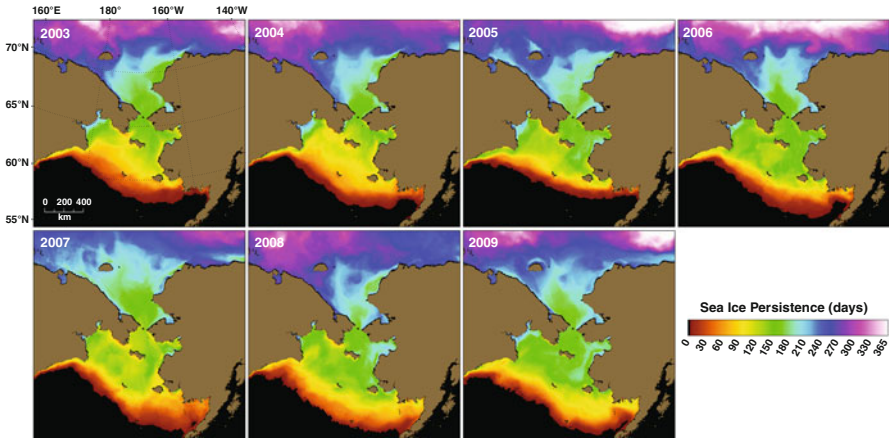


**Fig. 3.7** Annual sea ice persistence for the years 2003–2009 showing recent interannual variability in sea ice cover. Results are based on AMSR-E sea ice concentrations (using a 15 % sea ice concentration threshold)

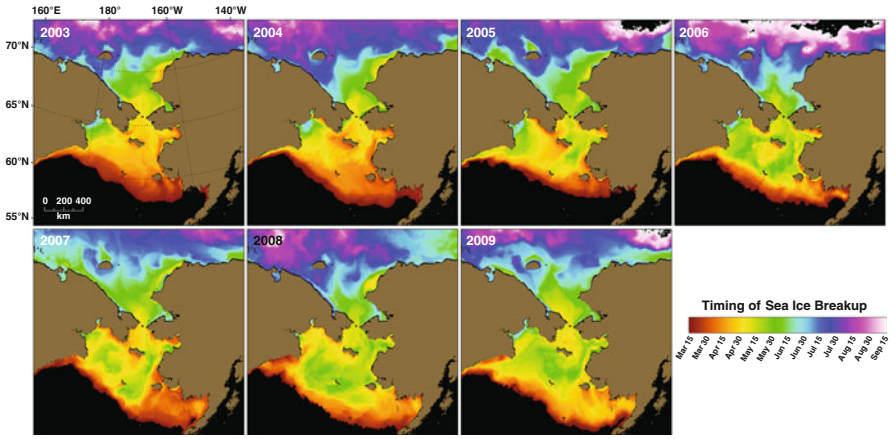


**Fig. 3.8** Recent interannual variability in the timing of sea ice breakup for the years 2003–2009. Results are based on AMSR-E sea ice concentrations (using a 15 % sea ice concentration threshold)

Sea typically breaking up in late April-early May and advancing into the northern Chukchi Sea by July or August. The progression of sea ice breakup from south to north across the entire PAR (from the Bering Sea to the Chukchi Sea) occurs over a ~6 month time span (from mid-March through mid-September).

Compared to patterns in sea ice breakup, the timing of sea ice formation is distinctly more homogenous across the PAR and more closely follows an ideal latitudinal gradient (Fig. 3.9). This likely occurs in part because sea ice variability associated with polynya opening events primarily occurs during late winter and

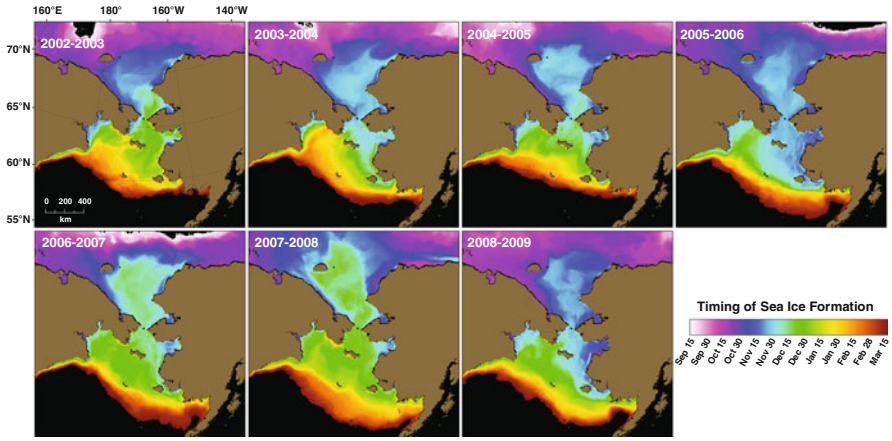


**Fig. 3.9** Recent interannual variability in the timing of sea ice formation for the years 2002–2009. Results are based on AMSR-E sea ice concentrations (using a 15 % sea ice concentration threshold)

spring (e.g., Fu et al. 2012), rather than during autumn and early winter with sea ice formation. Across the PAR, sea ice forms first in the northern Chukchi Sea during September and October, whereas much of the remainder of the region (including both the Bering and Chukchi Seas) forms sea ice slightly later and relatively quickly during November and December. The most southern portion of the ice edge in the Bering Sea (in the vicinity of St. Matthew Island) then slowly advances southward over a longer timeframe (January through March) before ice breakup begins again in the spring. Over the 7 years investigated here, the 2006–2007 and 2007–2008 seasons show distinctly later seasonal sea ice formation compared with the other years (Fig. 3.9). These two seasons bound the September 2007 minimum in observed sea ice cover across the Arctic Ocean. The later sea ice formation during the 2007–2008 season is likely the direct aftermath of the shortened duration of summer 2007 sea ice cover. In addition, a shorter ice-covered period during the previous 2006–2007 season could have contributed to a younger, thinner ice cover that was more susceptible to melt during the following summer of 2007. Further discussion of the recent variability in sea ice age and thickness is found in the following two sections (Sects. 3.3 and 3.4).

## 3.3 Sea Ice Age

### *3.3.1 Sea Ice Age Data and Analysis*

Recent decreases in summer sea ice extent (Sect. 3.2) not only affect total ice coverage but also have resulted in a fundamental change in the nature of the Arctic ice itself – the change from a largely perennial (multiyear) ice cover to a more seasonal

coverage dominated by first-year ice (Johannessen et al. 1999; Comiso 2002; Belchansky et al. 2004; Nghiem et al. 2006; Kwok 2007; Maslanik et al. 2007a, 2011; Kwok and Cunningham 2010). There are different ways of looking at this change: (a) the amount of multiyear vs. first-year ice, (b) which areas of the Arctic now experience periods of open water instead of continuous ice coverage, and (c) the characteristics of the surviving multiyear ice pack. Each of these carries different implications in terms of understanding how the Arctic Ocean is changing. Here, we consider how the ice cover has evolved since 1979 in terms of the amount and spatial coverage of first-year and multiyear ice in the PAR, and in terms of the age distribution within the category of multiyear ice.

We use sea ice "age" data prepared by Fowler et al. (2004; updated 2010), and described further by Maslanik et al. (2007a, 2011) and Stroeve et al. (2011). In brief, using satellite data and drifting buoys, it is possible to monitor the formation, movement, and disappearance of sea ice. This history can then be used to estimate ice age, as shown by Fowler et al. (2004) and Rigor and Wallace (2004). In the Fowler et al. (2004) approach, ice movement is calculated using a cross-correlation technique applied to sequential, daily satellite images acquired by the SMMR, SSM/I, and Advanced Very High Resolution Radiometer (AVHRR) sensors. Motion vectors are then blended via optimal interpolation with International Arctic Buoy Program drifting-buoy vectors. Using the resulting 12.5 km resolution Equal-Area Scalable Earth (EASE) grid of ice motion vector fields from 1979 onward, ice age can then be estimated by treating each grid cell that contains ice as an independent Lagrangian particle and transporting the particles at weekly time steps. The datasets are therefore similar to the buoy-derived age fields of Rigor and Wallace (2004), but provide additional spatial detail. If the passive microwave-derived ice concentration remains at least 40 %, then that particle is assumed to have survived summer melt and its age is incremented by 1 year. A second version of the product uses a 15 % concentration threshold to age ice in areas of the diffuse, marginal ice zone (Maslanik et al. 2011). Unless noted otherwise (e.g., Fig. 3.10), the 40 % concentration version of the age data is used for the analyses presented here. It is important to emphasize that with a 40 % concentration threshold (and even with the 15 % threshold), some ice may still be present. In the figures presented, these areas are specifically flagged as "<40 %" or "<15 %" rather than as "open water". When age classes are aggregated into first-year and multiyear (i.e., second-year and older ice) categories, the information is comparable to the passive and active microwave satellite-derived time series of first-year and multiyear ice analyzed in other multiple studies (Johannesen et al. 1999; Nghiem et al. 2006; Comiso et al. 2008; Kwok et al. 2010). See Fowler et al. (2004), Rigor and Wallace (2004), Maslanik et al. (2007a, 2011) and Stroeve et al. (2011) for further details.

### *3.3.2 Recent Variability in Sea Ice Age*

To place the changes in sea ice within the PAR into a broader context, Figs. 3.10 and 3.11 show the spatial and fractional coverage of ice age classes from 1985 through 2010 for the Arctic as a whole. The data capture the general trend seen in other

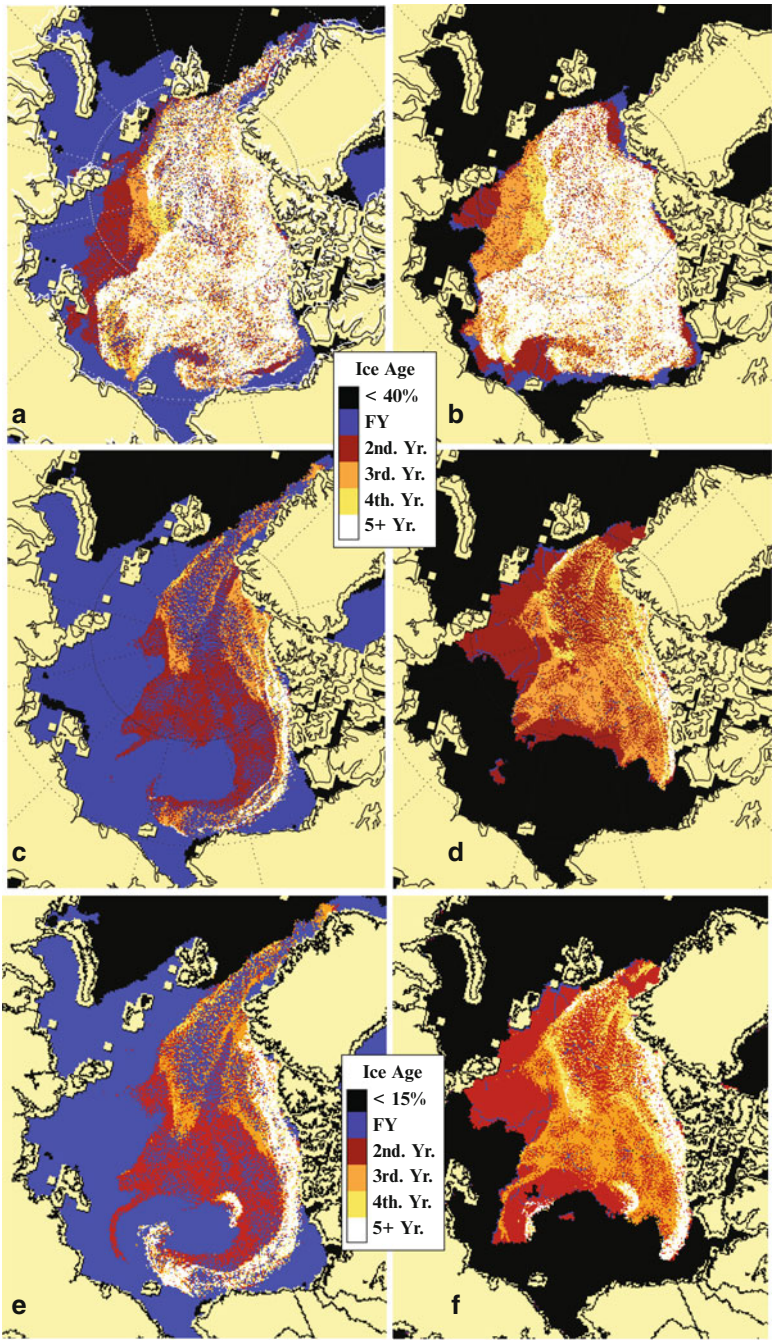


**Fig. 3.10** Distribution of sea ice of different ages for (**a**) mid-May 1985, (**b**) end of September 1985, (**c**) mid-May 2010, and (**d**) end of September 2010. Panels (**e**) and (**f**) show the 2010 age maps generated using a 15 % ice concentration threshold during mid-May and September, respectively

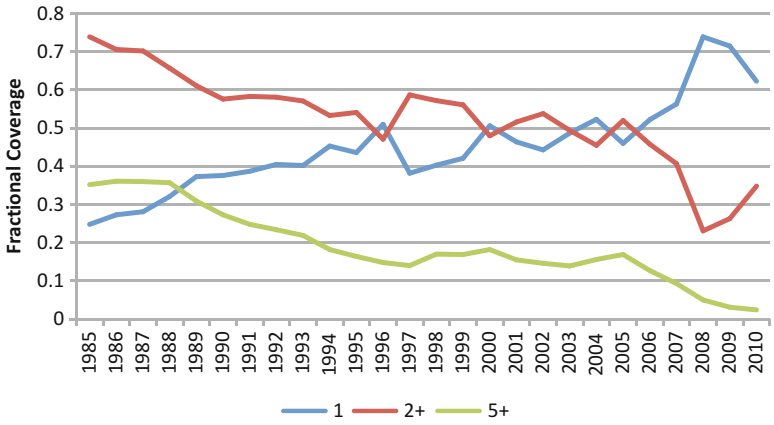


**Fig. 3.11** Fractional coverage of sea ice for different age ranges for mid-May 1985–2010. The geographic domain is the Arctic Ocean proper. First-year ice (*blue*), second-year and older ice (*red*), fifth-year ice and older (*green*)

studies of the overall loss in multiyear ice extent, but as discussed by Maslanik et al. (2007a, 2011), the overall reduction of the older multiyear ice types has been particularly large. In recent years, the multiyear ice in the Beaufort and Chukchi seas and Canada Basin is not ice that persists in the region from year to year, but instead is transported into the area each year from farther north and east by the clockwise motion of the Beaufort Gyre (e.g., Proshutinsky et al. 1997) replacing first-year ice that formed in the area following extensive retreats of the pack edge during summer melt. This sequence of summer ice retreat followed by replenishment of multiyear ice typifies conditions in recent years, as seen in panels c and d of Fig. 3.10. In summary, the ice over most of the Arctic Ocean basin is no longer dominated by perennial ice as it was prior to the late 1990s.

Shifts in the age structure of ice within the Arctic Ocean basin translate into significant interannual changes for the PAR. Ice conditions prior to melt onset (mid-May) and at the end of the summer melt period (end of September) for 1985 through 2010 for the PAR and four sub regions (Figs. 3.12, 3.13, 3.14 and 3.15) show a general trend of diminishing multiyear ice extent in the western Arctic, with a greatly reduced fraction of older age classes. Using the 40 % concentration version of the age data, there was a consistent loss in the oldest ice types from 1985 to 2010 (Fig. 3.15), with the oldest ice coverage decreasing from approximately 40 % of the ice pack in 1985 to less than 4 % in 2010 for May. For multiyear ice during May, the fractional coverage remained fairly stable from 1990 to 2001 but decreased markedly after 2009, reaching a minimum of 15 % in 2009 (or a net loss of ~80 % of the multiyear ice extent). The change in fractional coverage was slightly greater for September, with the multiyear ice coverage decreasing from ~80 % in 1985 to less than 30 % in 2010. Despite the fact that relatively little multiyear ice has survived summer melt in recent years in the PAR, multiyear ice of different age categories

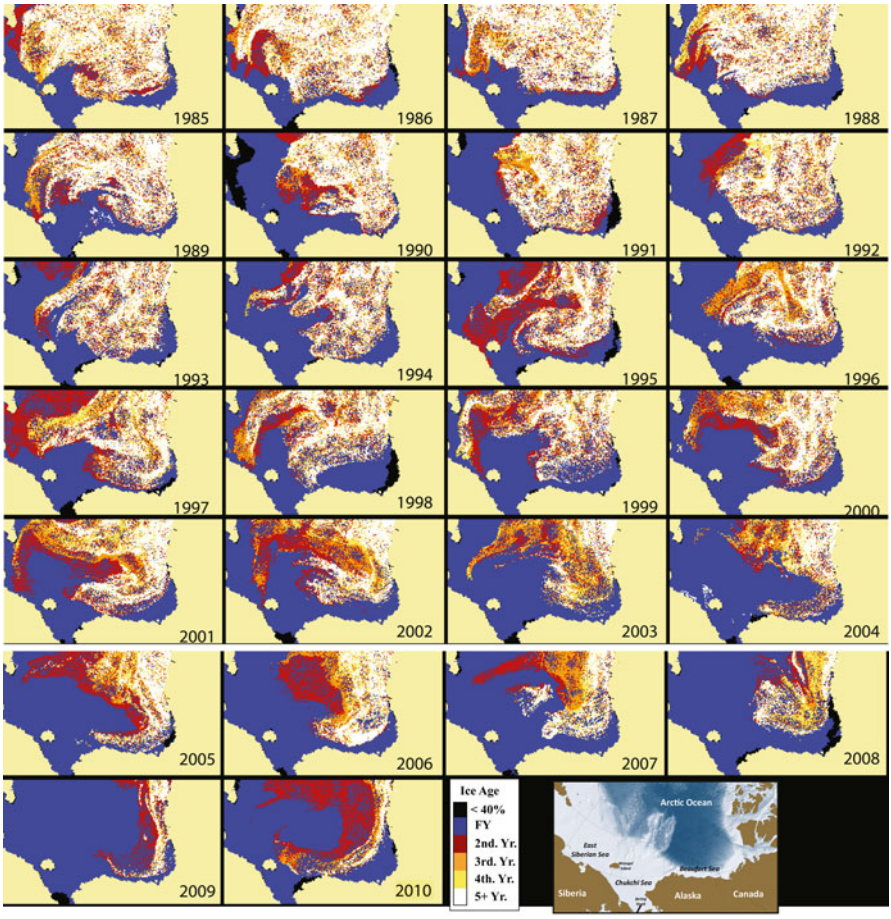


**Fig. 3.12** Fractional coverage sea ice by age category for the PAR for mid-May of 1985 through 2010

continues to be present in the area at other times of the year, via transport of multiyear ice from the north and east. This continued presence is more apparent when the minimum ice concentration threshold of 15 % is used (e.g., panels e and f of Fig. 3.10), which retains more of the diffuse, marginal ice cover.

While there is considerable interannual variability in ice conditions, two periods of substantial change can be seen. The first is a pronounced loss of multiyear ice in 1989 and 1990, associated with the extremely strong positive Arctic Oscillation (AO) that favored northward transport away from the Siberian Arctic (Rigor et al. 2002). The time series of ice age composition within sub-regions 1 and 3 of the PAR depict this well, particularly sub-region 1 (Fig. 3.16). While multiyear ice recovered somewhat through the late 1990s, it was younger overall and likely thinner (e.g., Maslanik et al. 2007a, 2011; Lindsay et al. 2009) than prior to 1989. The second

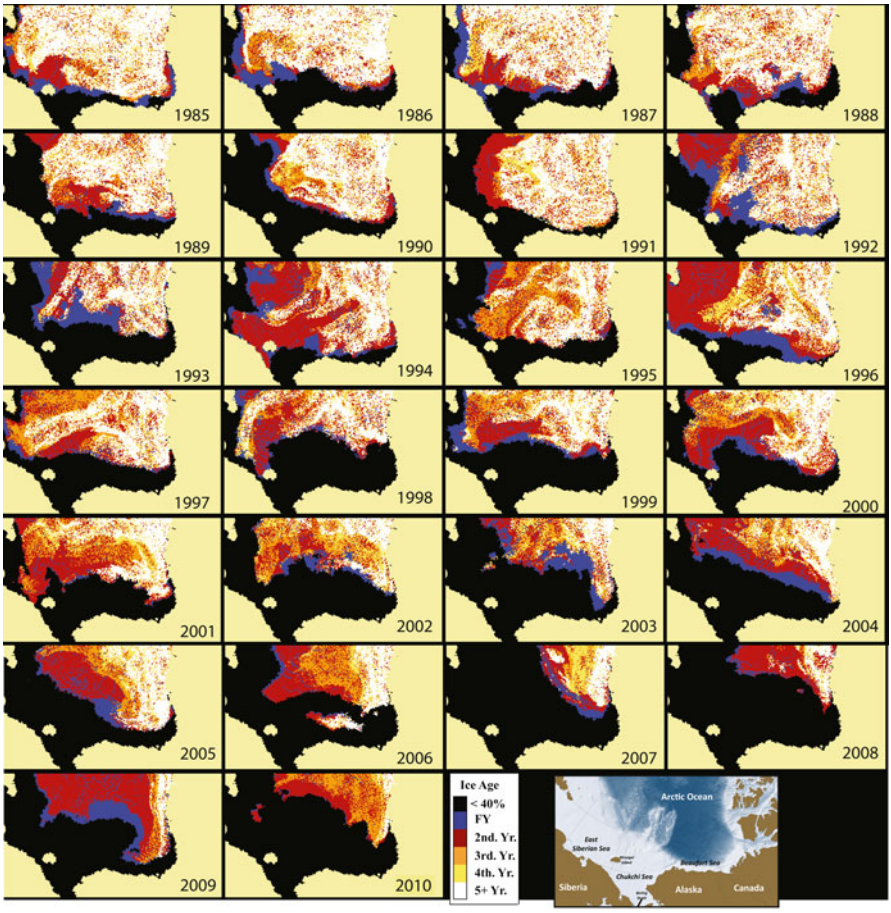


**Fig. 3.13** Fractional coverage sea ice by age category for the PAR for the end of September, 1985 through 2010. Note that the *black areas* indicate areas where passive microwave-derived ice concentration is less than 40 %, rather than indicating areas of 100 % open water

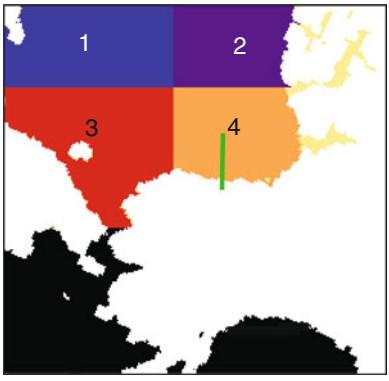


**Fig. 3.14** Geographic domain used for calculations of ice coverage by age category. The four individual regions are labeled 1–4. Land (*white*) and portions of the Canadian Archipelago (*yellow*) are excluded. The transect used for transport calculations (Fig. 3.17) is in *green*

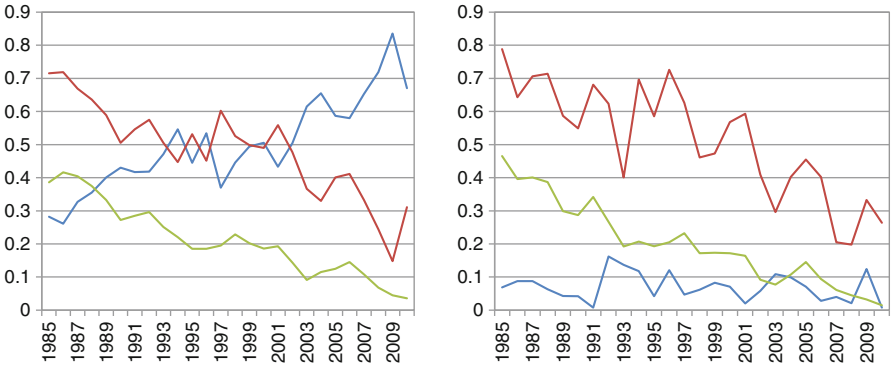


**Fig. 3.15** Fractional coverage of sea ice of different age ranges summarized over the full PAR (regions 1–4 in Fig. 3.14) for mid-May (*left panel*) and end of September (*right panel*). First-year ice (*blue*), second-year and older ice (*red*), fifth-year and older ice (*green*)

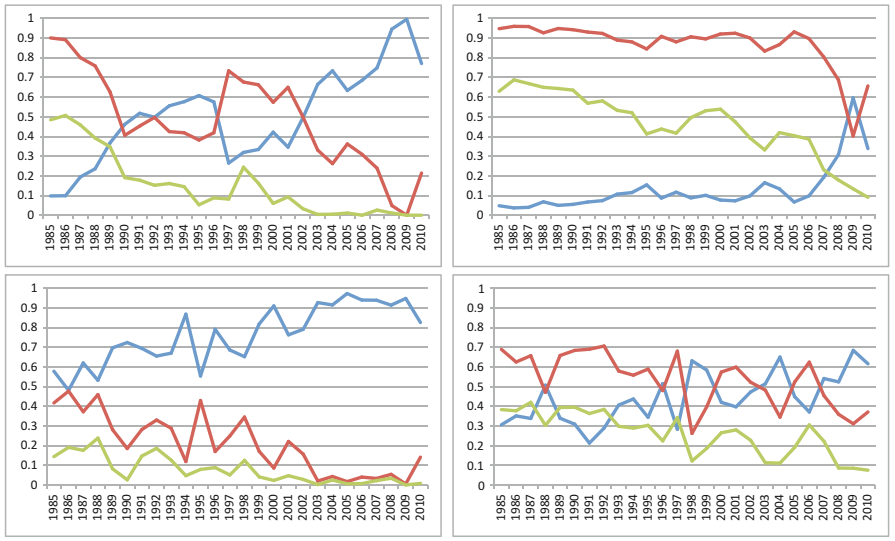


**Fig. 3.16** Fractional coverage of sea ice of different age ranges in mid-May for the four regions indicated in Fig. 3.14. Region 1 (*top left panel*), Region 2 (*top right*), Region 3 (*bottom left*), Region 4 (*bottom right*). First-year ice (*blue*), second-year and older ice (*red*), fifth-year and older ice (*green*)

notable period of change began in 2003, when atmospheric circulation patterns and perhaps changes in northward ocean heat transport (Maslanik et al. 2007b; Wang et al. 2009) diminished the multiyear ice from the western Beaufort and northern Chukchi Seas (as in sub-region 3 in Fig. 3.16). This likely occurred through a

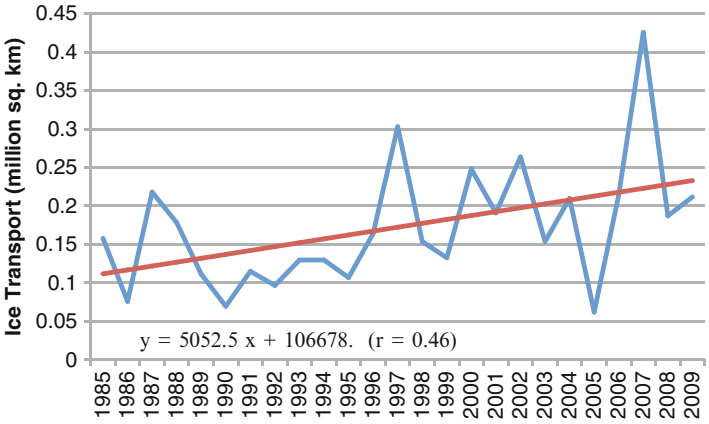


**Fig. 3.17** Annual ice transport during winter October–April across a north-south transect in the Beaufort Sea as indicated in Fig. 3.14. The values are for ice years (e.g., the value for 1985 spans October 1985–April 1986)

combination of northward ice drift and greater melt, but the specific contributions of the different mechanisms remain unclear.

In sub-region 4 (eastern Beaufort Sea), the pack ice has oscillated between being predominantly first-year vs. multiyear since 1997, before which it was mostly multiyear ice. The proportion of the multiyear pack that consists of the oldest ice types has remained relatively constant. The greater variability in the mixtures of ice types since 1997 is likely related to variability in east-to-west transport prior to the melt season. Calculation of ice transport (Fig. 3.17) across the transect location indicated in Fig. 3.14, estimated using satellite derived ice motion vectors (Stroeve et al. 2011) for October through April 1985–2009, shows considerable interannual variability but with a general trend toward greater transport in the latter years. Record transport was observed in Autumn 2009 through Winter 2010, in part accounting for the extensive westward drift of the tongue of multiyear ice seen in 2010 (Stroeve et al. 2011) and apparent in Fig. 3.12. Examining the time series of ice transport across the Beaufort Sea transect suggests that the record transport arose from strong, episodic wind-driven events rather than continuous uniform ice drift.

In sub-region 2 (eastern Canada Basin), although the oldest ice types have decreased over time, the multiyear ice coverage remained constant until 2007 indicating a shift to a younger multiyear pack. The extreme ice loss in summer 2007 was the first case in the satellite record where ice was removed throughout the entire western portion of the PAR. This has been followed by some recovery of the multiyear ice extent but as with the effects from the AO in 1990, the multiyear ice is younger than it was previously and may be less able to withstand summer melt (Lindsay et al. 2009).

## 3.4 Sea Ice Thickness

### *3.4.1 Sea Ice Thickness Data and Background*

While many previous studies have analyzed changes in ice extent and concentration (e.g. Comiso 2009; Stroeve et al. 2011), this section focuses on ice thickness as it gives a better indication of ice volume variability. Temporal changes in the Arctic sea ice thickness (or draft) have been noted by several investigators over the last few decades. McLaren (1989) compared 1958 ice draft measurements, obtained via acoustic profilers aboard the USS *Nautilus*, to similar measurements from the 1970 expedition of the USS *Queenfish*. The *Queenfish* resampled along the original *Nautilus* route across the Arctic Basin via the North Pole and thus provided a robust, yet snapshot, comparison between these two time periods. The mean draft decreased over the 12 years from 3.08 to 2.39 m (or by ~22 %). A reduction in the sea ice thickness north of Greenland was noted by Wadhams (1990) between 1976 and 1987. This reduction was found to be equivalent to at least a 15 % loss of volume over an area of 300,000 km$^2$. Rothrock et al. (1999) utilized data obtained via U.S. Navy submarines from the Scientific Ice Expeditions (SCICEX) of the 1990s and compared those with historic cruise datasets from 1958 to 1976. Geographically nearly overlapping samples from the end of the melt season averaged over five cruises during 1958–1976 (i.e. 1958, 1960, 1962, 1970, and 1976) were compared to similar averaged data from three cruises during the 1990s (i.e., 1993, 1996, and 1997) and reported a mean ice draft reduction of 1.3 m at the end of the melt season. This difference (from 3.1 m in 1958–1976 to 1.8 m in 1993–1997) represents a mean decline of 40 % over much of the deep-water portion of the Arctic Ocean.

Although many previous studies have shown reductions in the sea ice thickness of the Arctic Ocean, questions remained as to whether the true long-term trend could be distinguished from natural temporal and spatial variability using the available limited data. Rothrock et al. (2008) used all U.S. submarine data in the data release area (DRA, the region of U.S. Navy submarine data) from 1975 to 2000, along with multiple regression techniques, to separate the interannual change, the annual cycle, and the spatial field. The observed ice draft within the DRA showed declines from a maximum of 3.42 m in 1980 to 2.29 m in 2000 (and an overall 1.25 m decrease in ice thickness), with an observational error standard deviation of 0.38 m. Rothrock et al. (2008) noted a need for observations outside the DRA in order to assess the role of sea ice redistribution (i.e., with no or little change in the Arctic-wide sea ice volume; Holloway and Sou 2002) from the DRA into Russian waters or into the region south of the DRA and north of Canada. Because the DRA only encompasses ~38 % of the Arctic Ocean (Kwok and Rothrock 2009), sea ice thickness variability outside this region is still poorly known.

More recently, sea ice thickness has been estimated in the Arctic Ocean from satellite measurements of ice freeboard, which on average accounts for 10–15 % of ice thickness. Based on estimates of ice freeboard from satellite altimeter measurements

(ERS-1 and ERS-2), Laxon et al. (2003) demonstrated strong interannual thickness variability of the Arctic sea ice cover between 1993 and 2001. Haas (2004) showed a similar magnitude of interannual variability in the Transpolar Drift during 1991–2001 using independent measurements from drilling and electromagnetic (EM) sounding. Giles et al. (2008) reported on significant thinning of Arctic sea ice (0.49 m in the western Arctic) following the 2007 ice extent minimum based on the Envisat-derived sea ice thickness anomalies between 2002 and 2007. Kwok et al. (2009) compared ice thickness data estimated from the Ice, Cloud, and land Elevation Satellite (ICESat) autumn (mid-October to mid-November) and winter (late February to late March) campaigns during 2003–2008 with historic submarine sonar measurements (Rothrock et al. 1999). They showed a dramatic reduction in the wintertime sea ice thickness between 1980 (3.64 m) and 2008 (1.89 m) within the DRA (Kwok et al. 2009), which represents a thickness decline of 1.75 m during the last three decades. However, sea ice thickness estimates from ICESat depend on several not well known factors, including total freeboard, snow depth, and densities of snow, ice and seawater (e.g., Kwok et al. 2007; Kwok and Cunningham 2008).

Overall, observations of ice thickness are space and time-limited, and are not yet sufficient to diagnose long-term changes in Arctic sea ice volume. Ice thickness estimates derived from ice draft measurements by upward looking sonar from submarines and moorings are less uncertain than those derived from ice freeboard measured by satellites. However, ice draft data are not available basin-wide or long-term, while satellite data in practice are still limited to ice thickness anomalies relative to short-term means.

### *3.4.2 Sea Ice Thickness Model Description*

In this section, we present sea ice thickness results from a high-resolution (~9 km) pan-Arctic coupled ice-ocean model (Naval Postgraduate School Arctic Modeling Effort, NAME). The NAME coupled sea ice-ocean model consists of a regional adaptation of the Parallel Ocean Program (POP) and dynamic-thermodynamic sea ice models (Maslowski et al. 2004) configured at a horizontal grid spacing of 1/12° (or ~9 km). Such horizontal resolution permits calculation of flow through the narrow passes of the Aleutian Islands (Maslowski et al. 2008a) and straits of the northern Bering Sea (Clement et al. 2005). In the vertical direction, there are 45 vertical depth layers ranging from 5 m near the surface to 300 m at depth, with eight levels in the upper 50 m. The model domain is configured in a rotated spherical coordinate system to eliminate grid singularity at the North Pole and to minimize changes in grid cell area due to convergence of meridians with latitude. It contains the sub-polar North Pacific (including the Gulf of Alaska, the Sea of Japan and the Sea of Okhotsk), the Arctic Ocean, the Canadian Arctic Archipelago (CAA), the Nordic Seas and the sub-polar North Atlantic (see Fig. 3.1a of Maslowski et al. (2004) for model domain). Model bathymetry is derived from two sources: the ETOPO5 at 5-km resolution for the region south of 64°N and the International Bathymetric

Chart of the Arctic Ocean (IBCAO; Jakobsson et al. 2000) at 2.5-km resolution for the region north of 64°N. Daily climatological runoff from the Yukon River (and all other major Arctic rivers) is included in the model as a virtual freshwater flux at the river mouth. However, in the sub-polar regions (e.g., Gulf of Alaska, Hudson Bay, Baltic Sea) the freshwater flux from runoff is introduced by restoring the surface ocean level (5 m thick) to climatological (Polar Science Center Hydrographic Climatology, PHC; Steele et al. 2001) monthly mean salinity values over a monthly time scale (as a correction term to the explicitly calculated fluxes between the ocean and underlying atmosphere or sea ice).

The ocean model was initialized with climatological, three-dimensional temperature and salinity fields (PHC) and integrated for 48 years in a spinup mode. The production run, forced with realistic daily averaged European Centre for Medium-Range Weather Forecasts (ECMWF) interannual reanalysis and operational data, covers the 26-year time period from 1979 through 2004. Additional details on the model, including sea ice, have been provided elsewhere (Maslowski and Lipscomb 2003; Maslowski et al. 2004, 2008b). Results from the production run are used for the analyses, to validate against available observations of sea ice thickness, and to provide information where and when data are missing.

### *3.4.3 Sea Ice Thickness Model Validation*

In order to evaluate the skill of the model in representing sea ice thickness variability, its output has been compared to sea ice thickness data gathered during the last three decades (McNamara 2006; Whelan 2007). Those data sets include the draft measurements conducted by U.S. Navy submarines between 1979 and 2000, EM induction ice thickness measurements gathered using a helicopter by the Alfred Wegener Institute in April 2003, and data collected by NASA's ICESat satellite for 2003. The comparison with submarine and EM data is problematic for several reasons. The main problem is that the data and model output are at very different spatial resolutions: A typical sonar beam footprint ranges in diameter from 2.6 to 6 m and it collects data every 1 m along-track, whereas the model grid cell is about 9 km × 9 km (or ~85 km$^2$) and tends to remove values at either extreme. Assuming the sonar footprint diameter of 6 m, a 50 km cruise segment yields a 0.3 km$^2$ swath for the ULS dataset. The same 50 km segment results in a 1,390 km$^2$ swath when using the three grid cell wide model output comparison. Another problem is the large mismatch (up to three orders of magnitude) between the number of data points and the number of grid cells for any given distance. Finally, the time of the observations used in this work is known at least to the day, which is in marked contrast to the monthly average model output available for the analysis.

We focus here on a comparison with submarine data which was analyzed similarly to Rothrock et al. (2008), by averaging the ice thickness for each straight segment of the cruise (corresponding to a distance of 50 km or less) and assigning

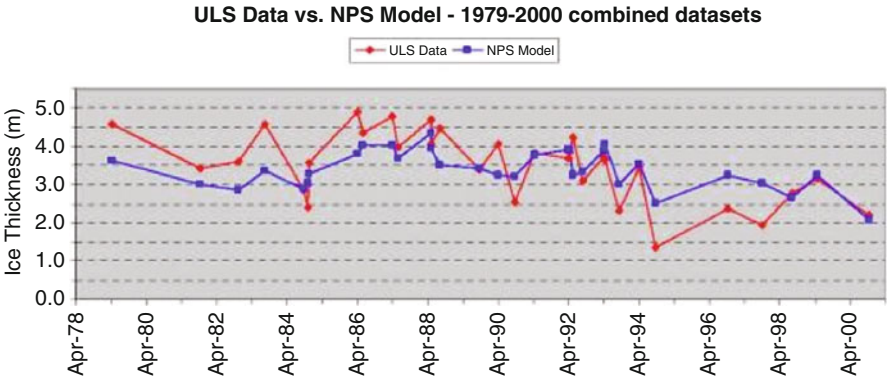


**Fig. 3.18** ULS weighted mean ice thickness (*red*) vs. NPS model weighted mean ice thickness (*blue*)

weights to the segments according to their lengths (McNamara 2006). The data were then binned into 10-cm ice thickness bins and plotted together as a probability distribution function (PDF) with y-axis values representing a percentage of points with a given ice thickness relative to the total number of points. This analysis allows comparison of both modal and mean ice thickness per cruise. A summary of mean ice thickness comparison from 32 submarine cruises is shown in Fig. 3.18. The NPS model performed reasonably well when comparing its sea ice thickness output to the ULS derived sea ice thickness measurements from the analyzed 32 submarine cruises. It showed practically no bias against data when examined across the record. However, the lack of sub-grid scale variations in ice thickness effectively contributed to a limited agreement with the data on very thin and very thick ice. This is evident in comparisons where the mean model thickness is in good agreement with the mean cruise thickness from the submarines. However, the modal distribution is not in good agreement, as it shows differences of order 0.5 m and/or missing thinner/thicker secondary modal maxima.

### *3.4.4 Recent Variability in Modeled Sea Ice Thickness*

Overall, modeled sea ice thickness has declined over the last few decades (Fig. 3.19). Mean September thickness in 1982 was in the range of 2.5–3.5 m over the central Arctic Ocean, with the thickest ice found along the northern coasts of the Canadian Archipelago and Greenland (Maslowski et al. 2007). Ten years later, the sea ice thickness in September 1992 was slightly thicker over much of the Arctic Ocean (Fig. 3.19b), although there was little change overall. In 2002, a dramatic reduction in sea ice thickness occurred with values <2 m across most of the central Arctic Ocean. Many marginal seas were ice-fee during this September time frame, in agreement with satellite observations. We also note the significant thinning of ice

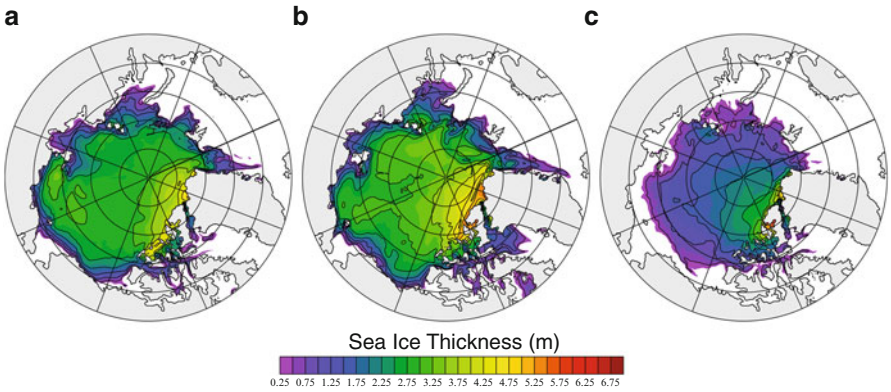


**Fig. 3.19** Modeled sea ice thickness (m) during September (**a**) 1982, (**b**) 1992, and (**c**) 2002

along the northern coasts of the Archipelago and Greenland. In addition, the tongue of ice that typically extends along the east coast of Greenland (above the East Greenland Current) was not present for the most part. The dramatic thinning described here is robust and independent of the strength of surface relaxation to climatological temperature and salinity, as shown by Maslowski et al. (2007). A shift in the mode (as defined by the highest percentage of total model grid cells per ice thickness bin) of ice thickness occurred during the mid-to-late 1990s (Fig. 3.20). The PDF shows that the mode prior to 1997 was in the range of 2.5–3.5 m thick. After that time, the mode was between 1.0 and 2.5 m thick – a strong shift toward thinner ice (Stroeve and Maslowski 2007). The reduction of the modal ice thickness represents the thinning of the multi-year pack ice toward the ice thickness range representative of first-year ice.

In light of the overall changes in Arctic sea ice thickness, we now focus on the changes in the Bering and Chukchi seas. The modeled mean ice thickness in the Chukchi Sea has declined throughout the seasonal cycle in a dramatic fashion since the late 1990s (Fig. 3.21). While the late summer/early autumn differences are the highest (~1 m for 1999–2003 and ~1.4 m in 2004), the wintertime changes are still noticeable (~0.5 m for 1999–2003), particularly in 2004 (~1 m). The seasonal cycle in the Bering Sea (Fig. 3.21), in contrast, shows much smaller changes (up to 0.15 m), with thinner ice occurring during the winter through early summer time frame in 2004. The only significant trends (over the 26-year time series) (Fig. 3.22, Table 3.2) in the Bering Sea ice thickness occur during June (−3.7 cm/decade) and July (−1.6 cm/decade). The Chukchi Sea ice thickness shows significant downward trends during June–December (Fig. 3.23, Table 3.2). The most severe ice thickness trends occur in September at −51.2 cm/decade, however early summer through early winter losses are all statistically significant and noteworthy (>25 cm/decade). Although the trends for January–May are not significant (at the 90 % level), sharp declines occur for all of these months beginning in 2001 (Fig. 3.23).

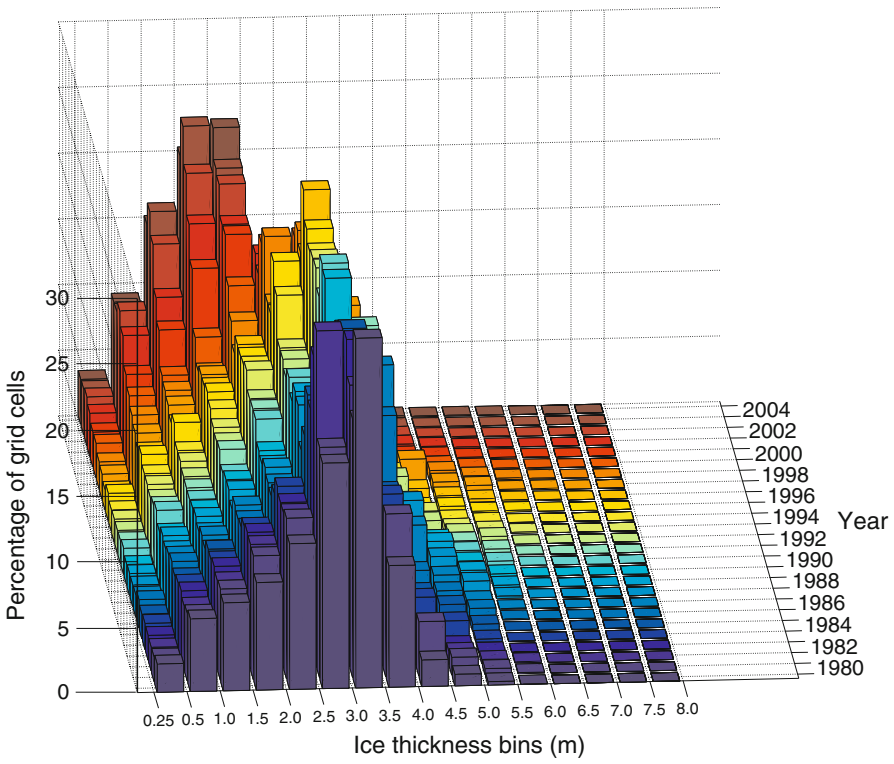


**Fig. 3.20** Probability distribution function (*PDF*) of modeled annual mean binned ice thickness (m). The *z*-axis shows percentage of the total model grid cells per thickness bin defined along the *x*-axis. The *y*-axis is time in years from 1979 to 2004 with a different color histogram for each year

### *3.4.5 Potential Mechanisms of Sea Ice Thinning*

Although many previous studies have shown reductions in the sea ice thickness of the Arctic Ocean (e.g., McLaren 1989; Wadhams 1990; Rothrock et al. 1999, 2008; Kwok et al. 2009) the direct cause(s) remain somewhat obscure. Rothrock et al. (1999) proposed three possible mechanisms for thinning the sea ice to the degree that was observed: (a) increased oceanic heat flux (additional 4 W $m^{-2}$), (b) increased poleward atmospheric heat transport (additional 13 W $m^{-2}$), or (c) increased downwelling shortwave radiation (additional 23 W $m^{-2}$). Still another possible cause of the thinning could be changes in precipitation and snow cover or advective processes such as sea ice export via Fram Strait. Rothrock et al. (1999) also noted all of these processes would be at the very limits of the present observational capability, and hence reaching a conclusion on the cause of the sea ice decline would prove difficult.

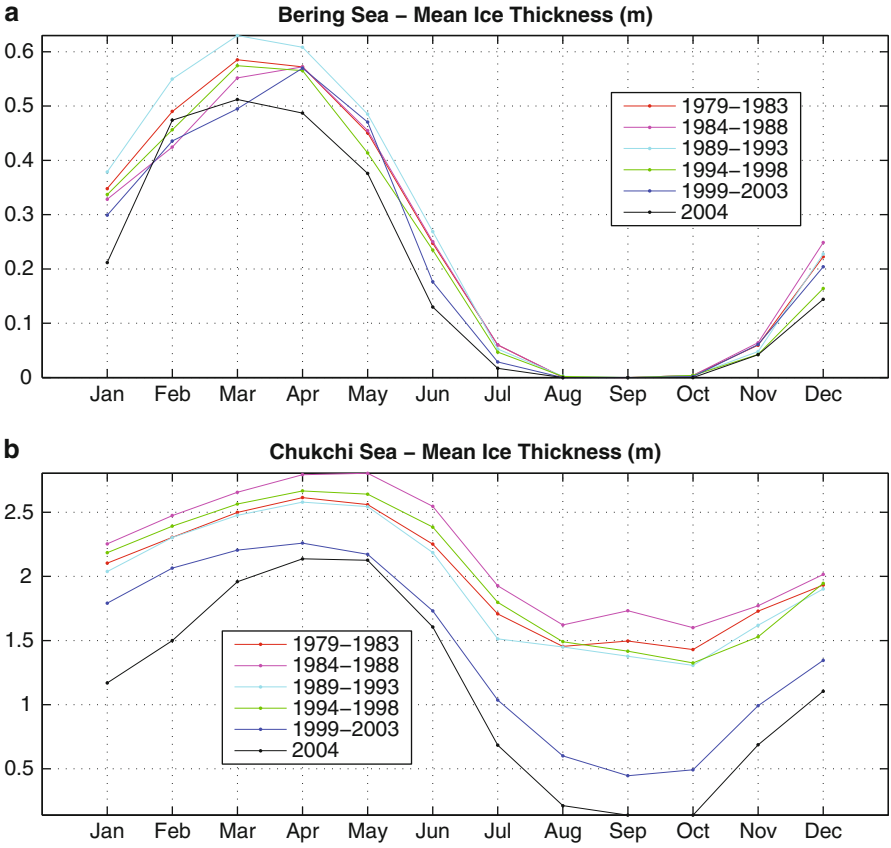


**Fig. 3.21** Monthly mean modeled sea ice thickness in 5-year periods (except for 2004) as shown in the legend for the (**a**) northern Bering Sea and (**b**) Chukchi Sea

Warming in the Arctic has been typically associated with high positive AO index (Rigor and Wallace 2004), however the recent accelerated warming in the late 1990s through 2000s has occurred under a relatively neutral AO regime, which poses important questions about the actual role of the AO in sea ice variability (Overland and Wang 2005). There is a clear indication that Arctic sea ice thickness has declined at a similar, if not faster, rate than that of ice extent/area. The overall decline in sea ice cover has been most prominent in the western Arctic, which implies that some of its causes might be related to summer Pacific water advected from the Bering Sea, over the Chukchi shelf, and into the deep Canada Basin (see Maslowski et al. 2014, this volume).

In the Chukchi Sea, the modeled ice thickness trends are the most severe during September (−51.2 cm/decade or −54.8 %/decade) (Table 3.2), which is, again, consistent with the observed sea ice extent trend in the same region for September (−63,840 km$^2$/decade or −31.8 %/decade) (Table 3.1). An earlier summer melt in

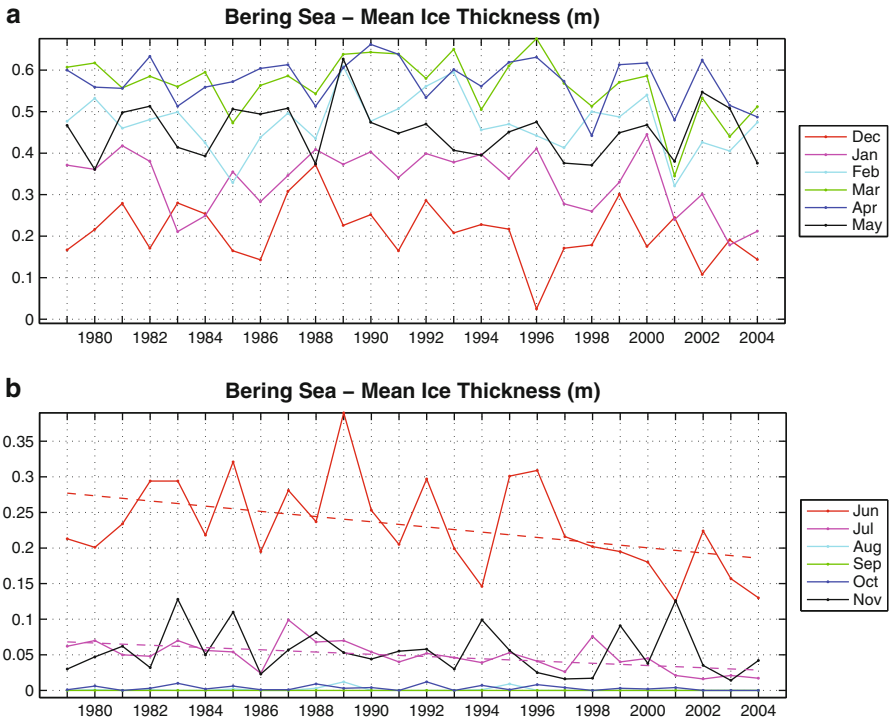


**Fig. 3.22** Monthly mean modeled sea ice thickness for 1979–2004 in the northern Bering Sea. Significant ($p<0.10$) linear trends are shown as *dashed lines* in the same color as the monthly mean values

**Table 3.2** Linear trends of modeled sea ice thickness decline in the Bering and Chukchi Seas over the 26 year time period (1979–2004). Only those trends that are statistically significant ($p<0.10$) are shown

| | Bering Sea | | Chukchi Sea | |
|---|---|---|---|---|
| | cm/decade | %/decade | cm/decade | %/decade |
| January | | | | |
| February | | | | |
| March | | | | |
| April | | | | |
| May | | | | |
| June | −3.7 | −17.4 | −27.6 | −12.0 |
| July | −1.6 | −25.8 | −34.7 | −20.1 |
| August | | | −40.2 | −39.3 |
| September | | | −51.2 | −54.8 |
| October | | | −46.7 | −60.1 |
| November | | | −37.8 | −26.9 |
| December | | | −28.3 | −16.3 |

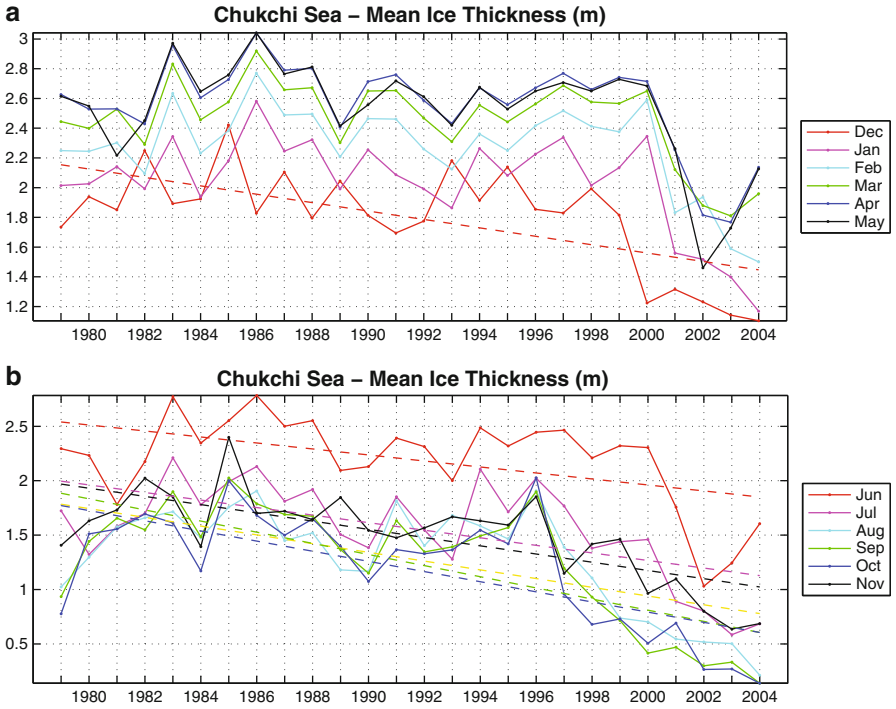


**Fig. 3.23** Monthly mean modeled sea ice thickness for 1979–2004 in the Chukchi Sea. Significant ($p<0.10$) linear trends are shown as *dashed lines* in the same color as the monthly mean values

the modeled sea ice thickness trends for the Bering Sea (Table 3.2) is consistent with observations, which also show declines in ice extent during June and July (Table 3.1). However, later sea ice formation (i.e., thinner ice during autumn) is not shown in the model results through 2004.

## 3.5 Implications and Possible Future States

Summer retreat of the sea ice pack tends to stop at the multiyear ice edge (i.e., first-year ice typically melts out more easily than multiyear ice), as is apparent for corresponding years in Figs. 3.12 and 3.13. As such, once multiyear ice is established it helps maintain ice extent. In other words, there tends to be two relatively stable states of sea ice: a seasonal ice state and a multiyear ice state. For example, once an area is converted to first-year ice, it tends to remain an area of seasonal ice cover, as happened during the late 1980s positive AO event. But if multiyear ice survives or re-captures a region, then it favors the multiyear ice state. However, since the late 1990s, even the oldest and likely thickest (e.g., Maslanik et al. 2007a) ice

transported into the Beaufort Sea has typically not survived through summer. The PAR has thus essentially become a region of multiyear ice loss, behaving more like a sub-arctic sea than the historical Arctic region dominated by perennial ice cover (Kwok and Cunningham 2010; Maslanik et al. 2011). An exception occurred in 2006, however, when a portion of multiyear ice in the Beaufort Sea consisting of the oldest ice types survived the melt season (Fig. 3.13). This suggests that while conditions have not been favorable for ice survival in recent years, they are likely close to a threshold in which favorable dynamic and thermodynamic conditions may allow extensive ice cover to survive through summer in the southern Beaufort Sea. Once a multiyear ice cover is re-established, it may act to maintain itself for several years, or until the next set of extreme conditions occurs (as in 1990 or 2007).

The tendency for the ice pack to melt back to the multiyear ice edge, along with the decreased survivability of multiyear ice in the southern Beaufort Sea, implies continued trends of more open water in the PAR. It is important to note that multiyear ice continues to be transported into the southern Beaufort Sea and occasionally farther west into the Chukchi Sea, causing some older ice types to be quite close to shore (Fig. 3.12). Unlike conditions in the 1980s and 1990s, the multiyear ice is now often confined to a relatively narrow band or tongue, with a tendency for the oldest and heaviest ice to be farthest south, with younger multiyear ice to the north transitioning to first-year ice. Some of the multiyear ice in the southern Beaufort Sea is among the oldest and thickest in the Arctic, so the potential exists to encounter multiyear ice during winter and throughout mid-summer in this region. In some cases, isolated multiyear floes can survive in the Beaufort and Chukchi seas throughout the melt season, possibly providing some isolated habitat for marine mammals and posing hazards for shipping.

While most of the ice pack might have now retreated well north of the continental shelf, it is possible that residual multiyear floes within the tongues of east-to-west transported multiyear ice might provide platforms useful for marine mammals and species across other trophic levels in relatively shallow water. However, the presence of a narrow band of heavy multiyear ice near shore might also give a false perception that heavy multiyear ice persists all the way to the North Pole. As such, any organism that assumed that ice north of the multiyear ice edge offshore of the Alaskan coast in recent years (particularly from 2004 onward) was perennial ice would in fact find itself over first-year ice and potentially a great distance from survivable ice once the summer melt season starts. In addition to ice extent, the nature of the ice itself in terms of the shift from a predominance of ice of several years of age to mainly first-year ice and young multiyear ice may have implications for biological processes and habitat. Ice characteristics such as thickness, salinity, snow cover, and surface and subsurface topography differ considerably between first-year and multiyear ice of different ages.

A decline in Arctic sea ice extent over the second half of the twentieth century was simulated by all of the global climate models participating in the Intergovernmental Panel of Climate Change Fourth Assessment Report (IPCC AR4) (Stroeve et al. 2007). However, the magnitude of satellite-observed negative trends in sea ice extent was not represented by the majority of models,

implying the models were too conservative. Possible causes presented by Stroeve et al. (2007 and references therein) included lack of a parameterization of sub-grid scale ice thickness distribution, as well as poor representation of modes of atmospheric variability, ocean circulation, heat convergence, and water column vertical structure. However, in general climate projections suggest that the ice pack will continue to transition toward a nearly entirely seasonal, first-year ice cover (e.g., Overland and Wang 2007; Douglas 2010; Wang et al. 2012). Even so, conditions might be similar to those observed in the last several years, with some multiyear ice persisting along the periphery of the Arctic Ocean adjacent to the high-latitude Canadian Archipelago coast. Some of this ice will be transported into the Canada Basin and Beaufort and Chukchi seas during the winter and as noted above, it would be scattered, low-concentration, residual areas of multiyear ice may or may not survive the melt season. The same situation may hold for the Canadian Archipelago channels, where residual multiyear ice might be transported into the passages during winter. As noted above, this could be significant for habitat and shipping, so the "ice free" summers projected by models might be better termed "nearly ice free". Also, over the coming decades, there will likely be periods (such as in 2010) when there is some recovery of the multiyear ice extent. However, it is likely that these will amount to periods of natural interannual variability superimposed on the overall long-term trend toward a nearly entirely seasonal ice cover. The tendency for two stable states of ice coverage (seasonal vs. multiyear) to persist may continue, with occasional extreme conditions promoting one ice state over the other. That being said, however, it seems that the nature of the extreme events favors a shift from thicker multiyear to thinner first-year ice rather than vice versa.

## 3.6 Summary

Sea ice across the Pacific Arctic Region (PAR) is highly seasonally variable, with sea ice existing only a few days each year in the most southern reaches of the sea ice zone of the northern Bering Sea, to nearly year-round coverage sea ice in the northern Chukchi Sea. Over the past several decades, the sea ice of the PAR has experienced some of the most dramatic changes in areal coverage, age, and thickness of the entire Arctic Ocean basin. The most extreme trends in sea ice cover across the PAR have occurred within portions of the Chukchi Sea, where annual sea ice persistence has declined by more than 30 days/decade over the 30 year record (1979–2008) of satellite observations. This decline results from earlier sea ice breakup (~10 days/decade earlier), and even more so by later sea ice formation (~20 days/decade later). In terms of sea ice age, the PAR has become a region of multiyear ice loss, behaving more like a sub-Arctic sea than the historical Arctic region dominated by perennial cover. The loss of multiyear ice is particularly striking in September, where the fractional coverage north of Bering Strait diminished from 80 % in 1985 to less than 30 % in 2010. Changes in sea ice thickness are

also most dramatic in the Chukchi Sea, with significant downward trends during June–December of 1979–2004. While September shows the highest trends in the Chukchi Sea (−51.2 cm/decade), recent sharp declines occur in all months beginning in 2001. Climate projections suggest that sea ice across the PAR will continue on a path toward a nearly entirely seasonal, first-year ice cover, which by its nature will be thinner and less seasonally persistent, with the possibility of some continued presence of multiyear ice through ridging and transport from the Arctic Basin to north of the Canadian Archipelago. As these trends continue, the changing sea ice will undoubtedly have profound impacts on ecosystem productivity across all trophic levels within the PAR.

**Acknowledgements** This research was in part supported by the NASA Cryospheric Sciences Program (Grant NNX10AH71G to K. Frey, and Grants NNX07AR21G and NNX11AI48G to J. Maslanik) and the NSF Arctic Sciences Division (Grants ARC-0804773 and ARC-1107645 to K. Frey, and Grant ARC-0712950 to J. Maslanik). P. Panday is thanked for assistance in satellite data processing. Funding support for the development, integration, and analyses of results from the NAME model (to W. Maslowski and J. Clement Kinney) was provided by multiple grants from the Arctic System Science (ARCSS) Program of the National Science Foundation, the Climate Change Prediction Program of the Department of Energy, and the Office of Naval Research. Computer resources were provided by the Department of Defense High Performance Computer Modernization Program (DOD/HPCMP).

## References

Arrigo KR, van Dijken GL (2011) Secular trends in Arctic Ocean net primary production. J Geophys Res 116:C09011. doi:10.1029/2011JC007151

Arrigo KR, Perovich DK, Pickart RS, Brown ZW, van Dijken GL, Lowry KE, Mills MM, Palmer MA, Balch WM, Bahr F, Bates NR, Benitez-Nelson C, Bowler B, Brownlee E, Ehn JK, Frey KE, Garley R, Laney SR, Lubelczyk L, Mathis J, Matsuoka A, Mitchell BG, Moore GWK, Ortega-Retuerta E, Pal S, Polashenski CM, Reynolds RA, Scheiber B, Sosik HM, Stephens M, Swift JG (2012) Massive phytoplankton blooms under Arctic sea ice. Science 336:1408. doi:10.1126/science.1215065

Belchansky GI, Douglas DC, Alpatsky IV, Paltonov NG (2004) Spatial and temporal multiyear sea ice distributions in the Arctic: a neural network analysis of SMM/I data, 1988–2001. J Geophys Res 109:C10017. doi:10.1029/2004JC002388

Cavalieri DJ, Parkinson CL, Vinnikov KY (2003) 30-year satellite record reveals contrasting Arctic and Antarctic decadal sea ice variability. Geophys Res Lett 30:1970. doi:10.1029/2003GL018031

Cavalieri D, Parkinson C, Gloersen P, Zwally HJ (2008) Sea ice concentrations from Nimbus-7 SMMR and DMSP SSM/I passive microwave data. National Snow and Ice Data Center, Boulder. Digital media

Clement JL, Maslowski W, Cooper L, Grebmeier J, Walczowski W (2005) Ocean circulation and exchanges through the northern Bering Sea – 1979–2001 model results. Deep Sea Res II 52:3509–3540. doi:10.1016/j.dsr2.2005.09.010

Comiso JC (2002) A rapidly declining perennial sea ice cover in the Arctic. Geophys Res Lett 29. doi:10.1029/2002GL015690

Comiso J (2009) Polar oceans from space, vol 41, Atmospheric and oceanographic sciences library. Springer, New York. doi:10.1007/978-0-387-68300-3

Comiso JC, Parkinson CL, Gersten R, Stock L (2008) Accelerated decline in the Arctic sea ice cover. Geophys Res Lett 35:L01703. doi:10.1029/2007GL031972

Douglas DC (2010) Arctic sea ice decline: projected changes in timing and extent of sea ice in the Bering and Chukchi Seas, U.S. Geological Survey open-file report 2010–1176. U.S. Department of the Interior/U.S. Geological Survey, Reston, 32 pp

Fowler C, Emery WJ, Maslanik J (2004) Satellite-derived evolution of Arctic sea ice age: October 1978 to March 2003. IEEE Geosci Remote Sens Lett 1:71–74. doi:10.1109/LGRS.2004.824741

Frey KE, Perovich DK, Light B (2011) The spatial distribution of solar radiation under a melting Arctic sea ice cover. Geophys Res Lett 38:L22501. doi:10.1029/2011GL049421

Fu H, Zhao J, Frey KE (2012) Investigation of polynya dynamics in the northern Bering Sea using greyscale morphology image-processing techniques. Int J Remote Sens 33:2214–2232. doi:10.1080/01431161.2011.608088

Giles KA, Laxon SW, Ridout AL (2008) Circumpolar thinning of Arctic sea ice following the 2007 record ice extent minimum. Geophys Res Lett 35:L22502. doi:10.1029/2008GL035710

Haas C (2004) Late-summer sea ice thickness variability in the Arctic Transpolar Drift 1991–2001 derived from ground-based electromagnetic sounding. Geophys Res Lett 31:L09402. doi:10.1029/2003GL019394

Holland MM, Bitz CM, Tremblay B (2006) Future abrupt reductions in the summer Arctic sea ice. Geophys Res Lett 33:L23503. doi:10.1029/2006GL028024

Holloway G, Sou T (2002) Has Arctic sea ice rapidly thinned? J Clim 15:1691–1701

Jakobsson M, Cherkis N, Woodward J, Macnab R, Coakley B (2000) New grid of Arctic bathymetry aids scientists and mapmakers. Eos Trans Am Geophys Union 81(9):89

Johannessen OM, Shalina EV, Miles MW (1999) Satellite evidence for an arctic sea ice cover in transformation. Science 286:1937–10939. doi:10.1126/science.286.5446.1937

Kahru M, Brotas V, Manzano-Sarabia M, Mitchell BG (2010) Are phytoplankton blooms occurring earlier in the Arctic? Glob Chang Biol. doi:10.1111/j.1365-2486.2010.02312.x

Kwok R (2007) Near zero replenishment of the Arctic multiyear sea ice cover at the end of 2005 summer. Geophys Res Lett 34:L05501. doi:10.1029/2006/GL028737

Kwok R, Cunningham GF (2008) ICESat over Arctic sea ice: estimation of snow depth and ice thickness. J Geophys Res 113:C08010. doi:10.1029/2008JC004753

Kwok R, Cunningham GF (2010) Contribution of melt in the Beaufort Sea to the decline in Arctic multiyear sea ice coverage: 1993–2009. Geophys Res Lett 37:L20501. doi:10.1029/2010GL044678

Kwok R, Rothrock DA (2009) Decline in Arctic sea ice thickness from submarine and ICESat records: 1958–2008. Geophys Res Lett 36:L15501. doi:10.1029/2009GL039035

Kwok R, Cunningham GF, Zwally HJ, Yi D (2007) Ice, Cloud, and land Elevation Satellite (ICESat) over Arctic sea ice: retrieval of freeboard. J Geophys Res 112:C12013. doi:10.1029/2006JC003978

Kwok R, Cunningham GF, Wensnahan M, Rigor I, Zwally HJ, Yi D (2009) Thinning and volume loss of the Arctic Ocean sea ice cover: 2003–2008. J Geophys Res 114:C07005. doi:10.1029/2009JC005312

Kwok R, Toudal Pedersen L, Gudmandsen P, Pang SS (2010) Large sea ice outflow into the Nares Strait in 2007. Geophys Res Lett 37:L03502. doi:10.1029/2009GL041872

Laxon S, Peacock N, Smith D (2003) High interannual variability of sea ice thickness in the Arctic region. Nature 425:947–950

Lindsay RW, Zhang J, Schweiger AJ, Steele MA, Stern H (2009) Arctic sea ice retreat in 2007 follows thinning trend. J Clim 22:165–176. doi:10.1175/2008JCLI2521

Maslanik J, Drobot S, Fowler C, Emery W, Barry R (2007a) On the Arctic climate paradox and the continuing role of atmospheric circulation in affecting sea ice conditions. Geophys Res Lett 34:L03711. doi:10.1029/2006GL028269

Maslanik JA, Fowler C, Stroeve J, Drobot S, Zwally J, Yi D, Emery W (2007b) A younger, thinner Arctic ice cover: increased potential for rapid, extensive sea-ice loss. Geophys Res Lett 34:L24501. doi:10.1029/2007GL032043

Maslanik J, Stroeve J, Fowler C, Emery W (2011) Distribution and trends in Arctic sea ice age through spring 2011. Geophys Res Lett 38:L13502. doi:10.1029/2011GL047735

Maslowski W, Lipscomb WH (2003) High-resolution simulations of Arctic sea ice during 1979–1993. Polar Res 22:67–74

Maslowski W, Marble D, Walczowski W, Schauer U, Clement JL, Semtner AJ (2004) On climatological mass, heat, and salt transports through the Barents Sea and Fram Strait from a pan-Arctic coupled ice-ocean model simulation. J Geophys Res 109:C03032

Maslowski W, Clement JL, Jakacki J (2007) Towards prediction of environmental Arctic change. Comput Sci Eng 9:29–34

Maslowski W, Clement Kinney J, DMarble DC, Jakacki J (2008a) In: Hecht MW, Hasumi H (eds) Ocean modeling in an eddying regime, vol 177, Geophysical monograph series., 350 pp

Maslowski W, Roman R, Kinney JC (2008b) Effects of mesoscale eddies on the flow of the Alaskan Stream. J Geophys Res 113:C07036. doi:10.1029/2007JC004341

McLaren AS (1989) The under-ice thickness distribution of the Arctic Basin as recorded in 1958 and 1970. J Geophys Res 94:4971–4983

McNamara TP (2006) Determination of changes in the state of the Arctic Icepack using the NPS pan-Arctic coupled ice-ocean model. MS thesis, Naval Postgraduate School, Monterey, CA. http://theses.nps.navy.mil/06Mar_McNamara.pdf

Nghiem SV, Chao Y, Neumann G, Li P, Perovich DK, Street T, Clemente-Colon P (2006) Depletion of perennial sea ice in the East Arctic Ocean. Geophys Res Lett 33:L17501. doi:10.1029/2006GL027198

Nghiem SV, Rigor IG, Perovich DK, Clemente-Colón P, Weatherly JW, Neumann G (2007) Rapid reduction of Arctic perennial sea ice. Geophys Res Lett 34:L19504. doi:10.1029/2007GL031138

Overland JE, Wang M (2005) The Arctic climate paradox: the recent decreases of the Arctic Oscillation. Geophys Res Lett 32:L06701. doi:10.1029/2004GL021752

Overland JE, Wang M (2007) Future regional Arctic sea ice declines. Geophys Res Lett 34:L17705. doi:10.1029/2007GL030808

Parkinson CL, Cavalieri DJ, Gloersen P, Zwally HF, Comiso JC (1999) Arctic sea ice extents, areas, and trends, 1978–1996. J Geophys Res 104:20837–20856

Perovich DK, Light B, Eicken H, Jones KF, Runciman K, Nghiem SV (2007) Increasing solar heating of the Arctic Ocean and adjacent seas, 1979–2005: attribution and role in the ice-albedo feedback. Geophys Res Lett 34:L19505. doi:10.1029/2007GL031480

Perovich D, Meier W, Maslanik J, Richter-Menge J (2011) Sea ice [in Arctic Report Card 2011]. http://www.arctic.noaa.gov/reportcard

Polyakov I et al (2007) Observational program tracks Arctic Ocean transition to a warmer state. Eos Trans Am Geophys Union 88(40):398. doi:10.1029/2007EO400002

Proshutinsky A, Yu A, Johnson MA (1997) Two circulation regimes of the wind-driven Arctic Ocean. J Geophys Res 102(C6):12493–12514

Rigor IG, Wallace JM (2004) Variations in the age of Arctic sea-ice and summer sea-ice extent. Geophys Res Lett 31:L09401. doi:10.1029/2004GL019492

Rigor IG, Wallace JM, Colony RL (2002) On the response of sea ice to the Arctic Oscillation. J Clim 15(18):2546–2663

Rothrock DA, Yu Y, Maykut GA (1999) Thinning of the Arctic sea-ice cover. Geophys Res Lett 26:3469–3472

Rothrock DA, Percival DB, Wensnahan M (2008) The decline in arctic sea-ice thickness: separating the spatial, annual, and interannual variability in a quarter century of submarine data. J Geophys Res 113:C05003. doi:10.1029/2007JC004252

Serreze MC, Maslanik JA, Scambos TA, Fetterer F, Stroeve J, Knowles K, Fowler C, Drobot S, Barry RG, Haran TM (2003) A record minimum arctic sea ice extent and area in 2002. Geophys Res Lett 30(3):1110. doi:10.1029/2002GL016406

Shimada K, Kamoshida T, Itoh M, Nishino S, Carmack E, McLaughlin F, Zimmermann S, Proshutinsky A (2006) Pacific Ocean inflow: influence on catastrophic reduction of sea ice cover in the Arctic Ocean. Geophys Res Lett 33:L08605. doi:10.1029/2005GL025624

Slagstad D, Ellingsen IH, Wassmann P (2011) Evaluating primary and secondary production in an Arctic Ocean void of summer sea ice: an experimental simulation approach. Prog Oceanogr 90:117–131

Spreen G, Kaleschke L, Heygster G (2008) Sea ice remote sensing using AMSR-E 89 GHz channels. J Geophys Res 113:C02S03. doi:10.1029/2005JC003384

Steele M, Morley R, Ermold W (2001) PHC: a global ocean hydrography with a high quality Arctic Ocean. J Clim 14:2079–2087

Steele M, Ermold W, Zhang J (2008) Arctic Ocean surface warming trends over the past 100 years. Geophys Res Lett 35:L02614. doi:10.1029/2007GL031651

Stroeve J, Maslowski W (2007) Arctic sea ice variability during the last half century. In: Brönnimann S, Luterbacher J, Ewen T, Diaz HF, Stolarski RS, Neu U (eds) Climate variability and extremes during the past 100 years. Springer, Dordrecht, pp 143–154

Stroeve JC, Serreze MC, Fetterer F, Arbetter T, Meier W, Maslanik J, Knowles K (2005) Tracking the Arctic's shrinking ice cover: another extreme September minimum in 2004. Geophys Res Lett 32. doi:10.1029/2004GL021810

Stroeve J, Holland MM, Meier W, Scambos T, Serreze M (2007) Arctic sea ice decline: faster than forecast. Geophys Res Lett 34:L09501. doi:10.1029/2007GL029703

Stroeve J, Serreze M, Drobot S, Gearheard S, Holland M, Maslanik J, Meier W, Scambos T (2008) Arctic sea ice extent plummets in 2007. Eos Trans Am Geophys Union 89(2):13. doi:10.1029/2008EO020001

Stroeve JC, Maslanik JA, Serreze MC, Rigor I, Meier W, Fowler C (2011) Sea ice response to an extreme negative phase of the Arctic Oscillation during winter 2009/2010. Geophys Res Lett 38:L02502. doi:10.1029/2010GL045662

Stroeve JC, Serreze MC, Holland MM, Kay JE, Maslanik J, Barrett AP (2012) The Arctic's rapidly shrinking sea ice cover: a research synthesis. Clim Chang 110:1005–1027

Wadhams P (1990) Evidence for thinning of the Arctic ice cover north of Greenland. Nature 345:795–797

Wang M, Overland JE (2009) A sea ice free summer Arctic within 30 years? Geophys Res Lett 36:L07502. doi:10.1029/2009GL037820

Wang J, Zhang J, Watanabe E, Ikeda M, Mizobata K, Walsh JE, Bai X, Wu B (2009) Is the Dipole Anomaly a major driver to record lows in Arctic summer sea ice extent? Geophys Res Lett 36:L05706

Wang M, Overland JE, Stabeno P (2012) Future climate of the Bering and Chukchi Seas projected by global climate models. Deep Sea Res Part II 65–70:46–57

Whelan J (2007) Understanding recent variability in the Arctic sea ice cover – synthesis of model results and observations. MS thesis, Naval Postgraduate School, Monterey, CA. https://edocs.nps.edu/npspubs/scholarly/theses/2007/Sep/07Sep_Whelan.pdf

Woodgate RA, Aagaard K, Weingartner TJ (2006) Interannual changes in the Bering Strait fluxes of volume, heat and freshwater between 1991 and 2004. Geophys Res Lett 33:L15609. doi:10.1029/2006GL026931

Zhang J (2005) Warming of the arctic ice-ocean system is faster than the global average since the 1960s. Geophys Res Lett 32:L19602. doi:10.1029/2005GL024216